

Geometric characterization of anomalous Landau levels of isolated flat bands

Yoonseok Hwang,^{1,2,3} Jun-Won Rhim,^{1,2,4,*} and Bohm-Jung Yang^{1,2,3,†}

¹Center for Correlated Electron Systems, Institute for Basic Science (IBS), Seoul 08826, Korea

²Department of Physics and Astronomy, Seoul National University, Seoul 08826, Korea

³Center for Theoretical Physics (CTP), Seoul National University, Seoul 08826, Korea

⁴Department of Physics, Ajou University, Suwon 16499, Korea

According to the Onsager's semiclassical quantization rule, the Landau levels of a band are bounded by its upper and lower band edges at zero magnetic field. However, there are two notable systems where the Landau level spectra violate this expectation, including topological bands and flat bands with singular band crossings, whose wave functions possess some singularities. Here, we introduce a distinct class of flat band systems where anomalous Landau level spreading (LLS) appears outside the zero-field energy bounds, although the relevant wave function is nonsingular. The anomalous LLS of isolated flat bands are governed by the cross-gap Berry connection that measures the wave-function geometry of multi bands. We also find that symmetry puts strong constraints on the LLS of flat bands. Our work demonstrates that an isolated flat band is an ideal system for studying the fundamental role of wave-function geometry in describing magnetic responses of solids.

I. INTRODUCTION

Geometry of Bloch wave functions, manifested in the quantities such as Berry curvature and Berry phase, is a central notion in modern description of condensed matter. Due to the significant role of the wave-function geometry in describing the fundamental properties of solids, finding efficient methods of measuring it has been considered as a quintessential problem in solid state physics. In this respect, examining the Landau level spectrum has received a particular attention, as one of the most efficient and convenient methods for detecting the geometric properties of Bloch states.

A conventional way of determining the Landau levels of Bloch states is to use the semiclassical approach based on the Onsager's semiclassical quantization rule given by

$$S_0(\epsilon) = \frac{2\pi eB}{\hbar} \left(n + \frac{1}{2} - \frac{\gamma_{\epsilon,B}}{2\pi} \right), \quad (1)$$

which is generally valid in weak field limit. Here $S_0(\epsilon)$ is the area of a closed semiclassical orbit at the energy ϵ in momentum space, B is magnetic field, e is the electric charge, \hbar is the reduced Planck constant, and n is a non-negative integer. The last term $\gamma_{\epsilon,B}$ indicates the quantum correction from Berry phase, orbital magnetization, etc. [1–5], reflecting the geometric properties of solids. A collection of discrete energies (ϵ) satisfying Eq. (1) forms the Landau levels which critically depend on the geometric quantity $\gamma_{\epsilon,B}$. For instance, in graphene with relativistic energy dispersion, Eq. (1) successfully predicts the \sqrt{nB} dependence of the Landau levels, where the existence of the zero-energy Landau level is a direct manifestation of the π -Berry phase of massless Dirac particles [6, 7]. Later, this semiclassical approach is generalized further to the cases with an arbitrary strength of magnetic field [8] where the zero-field energy dispersion in Eq. (1) is replaced by the magnetic band structure with B linear quantum corrections.

The Onsager's semiclassical scheme has provided a powerful method of understanding complicated Landau level spectra of solids intuitively. In usual dispersive bands where B linear quantum corrections are negligible in weak field limit, the Onsager's semiclassical approach in Eq. (1) predicts that the Landau levels are developed in the energy interval bounded by the upper and lower band edges of the zero-field band structure. However, there are few examples violating this expectation. Especially, several systems exhibit anomalous Landau levels appearing in gapped regions away from the zero-field energy bounds where the semiclassical orbit as well as $S_0(\epsilon)$ cannot be defined, according to Eq. (1). One famous example is the Landau levels of a Chern band which appear in an adjacent energy gap at zero-field. Similar behavior was also recently predicted in fragile topological bands characterized by nonzero Euler numbers [9–11]. More recently, it was shown that anomalous Landau levels also appear in singular flat bands [12, 13] where a flat band is crossing with another parabolic band at a momentum [14]. Interestingly, it is found that the Landau levels of a singular flat band appear in the energy region with vanishing density of states at zero magnetic field. Moreover, the total energy spreading of the flat band's Landau levels, dubbed the Landau level spreading (LLS), is solely determined by a geometric quantity, called the maximum quantum distance which characterizes the singularity of the relevant Bloch wave function [14].

In this work, we propose a distinct class of flat-band systems that exhibit anomalous Landau level structures. The flat band we consider is isolated from other bands by a gap, which we call an isolated flat band (IFB). An IFB is generally nonsingular as well as topologically trivial [15–17] as opposed to nearly flat topological bands or degenerate flat bands [18, 19], so that it does not belong to any category of the systems exhibiting anomalous Landau levels discussed above. However, it is found that the Landau levels of IFBs are anomalous, that is, unbounded by the original band structure at zero magnetic field and developed in the band gaps above and below the flat band.

In fact, the Onsager's semiclassical quantization rule in Eq. (1) generally does not work in flat bands, unless the B linear quantum corrections are properly included. This is be-

* Electronic address: jwrhim@ajou.ac.kr

† Electronic address: bjyang@snu.ac.kr

cause there are infinitely many semiclassical orbits allowed so that $S_0(\epsilon)$ cannot be uniquely determined. Interestingly, after taking into account the B linear quantum corrections, we find that an IFB generally exhibits anomalous LLS, and the upper and lower energy bounds for the LLS are determined by the cross-gap Berry connection defined as

$$A_i^{nm}(\mathbf{k}) = i\langle u_n(\mathbf{k}) | \partial_i u_m(\mathbf{k}) \rangle \quad (n \neq m), \quad (2)$$

where $u_n(\mathbf{k})$ is the periodic part of the Bloch wave function of the n -th band [20]. This is a multi-band extension of the conventional Abelian Berry connection and describes inter-band couplings. Let us note that, unlike the Abelian Berry connection defined for a single band, the cross-gap Berry connection $A_i^{nm}(\mathbf{k})$ ($n \neq m$) is gauge-covariant. We will show that the LLS of an IFB is given by the product of the x and y components of the cross-gap Berry connection between the flat band and other bands weighted by their energy. The LLS of an IFB is strongly constrained by the symmetry of the system, which is demonstrated in various flat band models including the Lieb and the Tasaki models as well as the model describing twisted bilayer graphene (see Results and Supplementary Note 4). Our work demonstrates the fundamental role of wave-function geometry in describing the Landau levels of flat bands.

II. RESULTS

A. Modified band dispersion and the Landau level spreading

The original Onsager's semiclassical approach predicts IFBs inert under external magnetic field, and thus it cannot explain the LLS of IFBs. On the other hand, the *modified semiclassical approach* developed by M.-C. Chang and Q. Niu [8] can resolve this problem. Contrary to the Onsager's approach, where the band structure at zero magnetic field $\varepsilon_n(\mathbf{k})$ is used to define the closed semiclassical orbits and the corresponding area $S_0(\epsilon)$, the modified semiclassical approach employs the modified band structure given by

$$E_{n,B}(\mathbf{k}) = \varepsilon_n(\mathbf{k}) + \mu_n(\mathbf{k})B, \quad (3)$$

where $\mathbf{B} = B\hat{\mathbf{z}}$ is the magnetic field, n is the band index, and $\mu_n(\mathbf{k})$ is the orbital magnetic moment of the n -th magnetic band in the z -direction arising from the self-rotation of the corresponding wave packet [8]. The explicit form of $\mu_n(\mathbf{k})$ is

$$\mu_n(\mathbf{k}) = \frac{e}{\hbar} \text{Im} \langle \partial_x u_n(\mathbf{k}) | [\varepsilon_n(\mathbf{k}) - H(\mathbf{k})] | \partial_y u_n(\mathbf{k}) \rangle, \quad (4)$$

where $H(\mathbf{k})$ is the Hamiltonian in momentum space and $\partial_i = \partial_{k_i}$ ($i = x, y$). Hence, the second term on the right-hand side of Eq. (3) indicates the leading energy correction from the orbital magnetic moment coupled to the magnetic field. In usual dispersive bands, the B -linear quantum correction is negligibly small in weak magnetic field limit compared to the zero-field band-width. This is the reason why the original Onsager's semiclassical scheme in Eq. (1) works well.

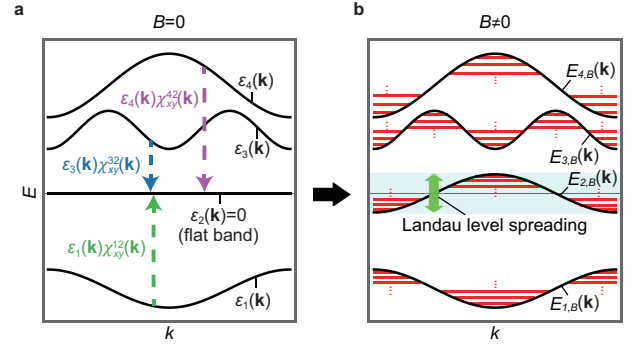


FIG. 1. **Landau level spreading (LLS) of an isolated flat band (IFB).** **a** The band structure of a two-dimensional system in the absence of magnetic field. The second band with the energy $\varepsilon_2(\mathbf{k}) = 0$ corresponds to the IFB. The inter-band coupling $\varepsilon_m(\mathbf{k})\chi_{xy}^{m2}(\mathbf{k})$ of the IFB with the other dispersive band of the energy $\varepsilon_m(\mathbf{k})$ ($m = 1, 3, 4$) is indicated by a dashed vertical arrow. **b** The modified band dispersion $E_{n,B}(\mathbf{k})$ ($n = 1, \dots, 4$) in the presence of the magnetic field. The corresponding Landau levels are shown by red solid lines. The LLS of the IFB is represented by the green arrow.

In the case of a flat band with zero band-width, on the other hand, the B -linear quantum correction always dominates the modified band structure $E_{n,B}(\mathbf{k})$ in Eq. (3) even in weak magnetic field limit. Moreover, the modified band dispersion of an IFB is generally dispersive so that the relevant semiclassical orbits can be defined unambiguously. As a result, one can obtain the Landau levels of the IFB in the adjacent gapped regions by applying the semiclassical quantization rule to $E_{n,B}(\mathbf{k})$, which naturally explains the LLS of the IFB. Especially, around the band edges of $E_{n,B}(\mathbf{k})$, one can define the effective mass m^* , which is inversely proportional to B , from which the Onsager's scheme predicts Landau levels with a spacing $\hbar e B / m^* \propto B^2$. The resulting Landau spectrum is bounded by the upper and lower band edges of $E_{n,B}(\mathbf{k})$. The total magnitude Δ of the LLS is determined by the difference between the maximum and the minimum values of $E_{n,B}(\mathbf{k})$, namely, $\Delta = \max E_{n,B}(\mathbf{k}) - \min E_{n,B}(\mathbf{k})$. This result is valid as long as the band gap E_{gap} between the IFB and its neighboring band at zero magnetic field is large enough, i.e., $E_{\text{gap}} \gg \max |E_{n,B}(\mathbf{k})|$. The generic behavior of an IFB under magnetic field is schematically described in Fig. 1 where one can clearly observe that the Landau levels of the IFB spread into the gaps at zero-field above and below the IFB.

B. Geometric interpretation of the LLS

Interestingly, we find that the LLS of IFBs is a manifestation of the non-trivial wave-function geometry of the flat band arising from inter-band couplings. One can show that the modified band dispersion of the IFB is given by

$$E_{n,B}(\mathbf{k}) = -2\pi \frac{\phi}{\phi_0} \frac{1}{A_0} \text{Im} \sum_{m \neq n} \varepsilon_m(\mathbf{k}) \chi_{xy}^{nm}(\mathbf{k}), \quad (5)$$

in which

$$\begin{aligned}\chi_{ij}^{nm}(\mathbf{k}) &= \langle \partial_i u_n(\mathbf{k}) | u_m(\mathbf{k}) \rangle \langle u_m(\mathbf{k}) | \partial_j u_n(\mathbf{k}) \rangle \\ &= A_i^{nm}(\mathbf{k})^* A_j^{nm}(\mathbf{k}),\end{aligned}\quad (6)$$

where $\phi_0 = h/e$, $\phi = BA_0$ is the magnetic flux per unit cell, and A_0 is the unit cell area assumed to be $A_0 = 1$. Here, we assume that the n -th band is the IFB at the zero energy without loss of generality so that $\varepsilon_m(\mathbf{k})$ in Eq. (5) should be interpreted as the energy of the m -th band with respect to the flat band energy. We note that $A_i^{nm}(\mathbf{k})$ indicates the cross-gap Berry connection between the n -th and m -th bands ($n \neq m$) defined in Eq. (2), and $\chi_{ij}^{nm}(\mathbf{k})$ is the corresponding fidelity tensor that describes the transition amplitude between the n -th and m -th bands as discussed below. See Supplementary Note 1 for the detailed derivation of Eq. (5). Hence, Eq. (5) indicates that the modified band dispersion of the IFB is given by the summation of the transition amplitudes $\chi_{xy}^{nm}(\mathbf{k})$ between the IFB and the m -th band weighted by the energy $\varepsilon_m(\mathbf{k})$ of the m -th band as illustrated in Fig. 1. This means that the immobile carriers with infinite effective mass in an IFB can respond to external magnetic field through the inter-band coupling, characterized by the cross-gap Berry connection, to dispersive bands. The geometric character of the LLS is evident in our interpretation based on Eq. (5).

Let us discuss the geometric character of the fidelity tensor $\chi_{xy}^{nm}(\mathbf{k})$ more explicitly. In general, the geometry of the quantum state $u_n(\mathbf{k})$ can be derived from the Hilbert-Schmidt quantum distance [21–23] defined as

$$s(u_n(\mathbf{k}), u_n(\mathbf{k}')) = 1 - |\langle u_n(\mathbf{k}) | u_n(\mathbf{k}') \rangle|^2, \quad (7)$$

which measures the similarity between $u_n(\mathbf{k})$ and $u_n(\mathbf{k}')$. For $\mathbf{k}' = \mathbf{k} + d\mathbf{k}$, we obtain

$$s(u_n(\mathbf{k}), u_n(\mathbf{k} + d\mathbf{k})) = \mathfrak{G}_{ij}^n(\mathbf{k}) dk_i dk_j, \quad (8)$$

where $\mathfrak{G}_{ij}^n(\mathbf{k})$ indicates the quantum geometric tensor [24–26] whose explicit form is

$$\begin{aligned}\mathfrak{G}_{ij}^n(\mathbf{k}) &= \sum_{m \neq n} \langle \partial_i u_n(\mathbf{k}) | u_m(\mathbf{k}) \rangle \langle u_m(\mathbf{k}) | \partial_j u_n(\mathbf{k}) \rangle \\ &= \sum_{m \neq n} \chi_{ij}^{nm}(\mathbf{k}),\end{aligned}\quad (9)$$

which shows that the quantum geometric tensor $\mathfrak{G}_{ij}^n(\mathbf{k})$ of the n -th band is given by the summation of the fidelity tensor $\chi_{ij}^{nm}(\mathbf{k})$ over all $m \neq n$. We note that $\chi_{ij}^{nm}(\mathbf{k})$ itself

cannot define a distance as the triangle inequality is not satisfied. However, it is related to the transition probability or the fidelity $F(u_n(\mathbf{k}), u_m(\mathbf{k}'))$ between the n -th and m -th bands [27] through the following relations:

$$F(u_n(\mathbf{k}), u_m(\mathbf{k}')) = |\langle u_n(\mathbf{k}) | u_m(\mathbf{k}') \rangle|^2, \quad (10)$$

$$F(u_n(\mathbf{k}), u_m(\mathbf{k} + d\mathbf{k})) = \chi_{ij}^{nm}(\mathbf{k}) dk_i dk_j. \quad (11)$$

Thus, the geometric interpretation based on Eqs. (5) and (11) clearly shows that the LLS originates from the inter-band coupling.

C. Symmetry constraints on the LLS

The LLS of an IFB is strongly constrained by symmetry. First, we consider a generic symmetry σ whose action on the Hamiltonian is given by

$$U_\sigma(\mathbf{k}) \overline{H(\mathbf{k})}^s U_\sigma(\mathbf{k})^\dagger = p H(O_\sigma \mathbf{k}), \quad (12)$$

where $s \in \{0, 1\}$, $p \in \{-1, 1\}$, and $U_\sigma(\mathbf{k})$ and O_σ are a unitary and orthogonal matrices representing σ , respectively. $\bar{x}^{s=1}$ denotes the complex conjugation of x while $\bar{x}^{s=0} = x$. Note that $s = 0$ and 1 are relevant to the unitary and anti-unitary symmetries, respectively, while $p = -1$ and $+1$ correspond to anti-symmetry and symmetry, respectively.

Among all possible symmetries of the form in Eq. (12), we find that the modified band dispersion $E_{n,B}(\mathbf{k})$ vanishes when the system respects the chiral C or space-time-inversion I_{ST} symmetries in the zero magnetic flux (see Methods and Supplementary Notes 2 and 3 for the detailed derivation). C and I_{ST} are characterized by $(O_\sigma, s, p) = (\mathbb{1}, 0, -1)$ and $(\mathbb{1}, 1, 1)$, respectively, where $\mathbb{1}$ is the identity matrix. In the following, we demonstrate that the LLS is proportional to B^2 for a flat-band system with I_{ST} symmetry in the zero magnetic field, while the LLS is forbidden in the presence of chiral symmetry. Interestingly, although I_{ST} symmetry would be broken as the magnetic field is turned on, the LLS is strongly constrained by I_{ST} symmetry.

We further find that $\max E_{n,B}(\mathbf{k}) = -\min E_{n,B}(\mathbf{k})$ when the system respects a symmetry satisfying $(-1)^s p \text{Det} O_\sigma = -1$ and $O_\sigma \neq \mathbb{1}$, such as time-reversal T or reflection R symmetry, at the zero magnetic field (see Methods and Supplementary Note 2 for detailed derivations). This implies that the minimum and maximum values of the LLS have the same magnitude but with the opposite signs. The relevant tight-binding models are shown in the Supplementary Note 4.

D. Generic flat-band systems

We first consider the spin-orbit-coupled (SOC) Lieb model [28] as an example of generic flat-band systems. The lattice structure for this model is shown in Fig. 2a. The model consists of the nearest neighbor hopping with the amplitude 1 and the spin-orbit coupling between the next nearest neighbor sites, which are denoted as green solid and dashed arrows, respectively,

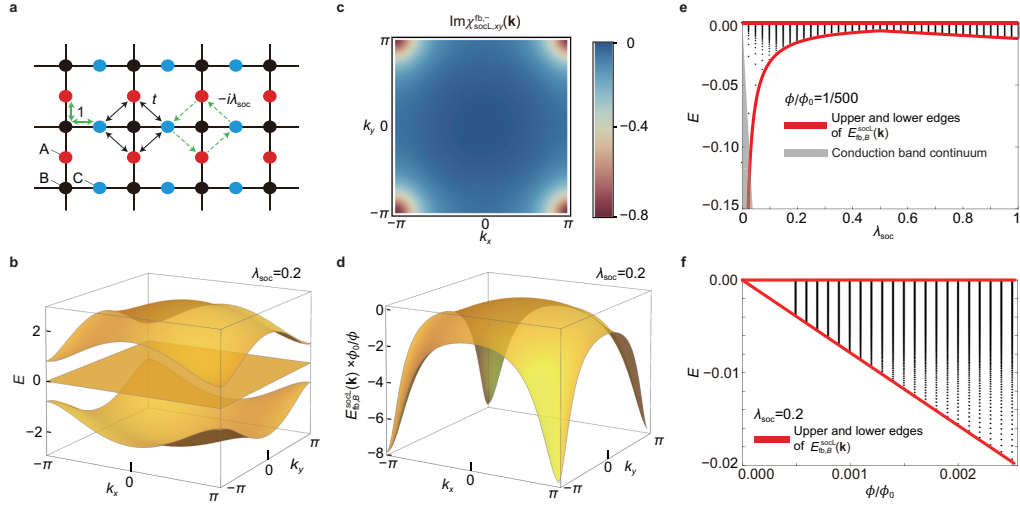


FIG. 2. **Landau level spreading of a generic system with an IFB.** **a** Lattice structure for the spin-orbit-coupled (SOC) Lieb model composed of three sublattices, A , B and C . The double-headed green arrows denote the nearest neighbor hoppings, and the single-headed green arrows indicate the spin-orbit coupling between A and C sublattices. The next-nearest hoppings t between A and C is set to be zero ($t = 0.0$) in the SOC Lieb model. **b** The band structure of $H_{\text{socL}}(\mathbf{k})$ with $\lambda_{\text{soc}} = 0.2$. **c** Distribution of $\text{Im} \chi_{\text{socL},xy}^{\text{fb},-}(\mathbf{k})$. Note that $\text{Im} \chi_{\text{socL},xy}^{\text{fb},-}(\mathbf{k}) = -\text{Im} \chi_{\text{socL},xy}^{\text{fb},+}(\mathbf{k})$. **d** The modified band dispersion $E_{\text{fb},B}^{\text{socL}}(\mathbf{k})$ of the flat band in the presence of magnetic flux. **e** Landau level spectra of the flat band (black dots) as a function of λ_{soc} for magnetic flux $\phi/\phi_0 = 1/500$. **f** Landau level spectra of the flat band (black dots) as a function of magnetic flux ϕ/ϕ_0 for $\lambda_{\text{soc}} = 0.2$.

in Fig. 2a. The tight-binding Hamiltonian in momentum space is given by

$$H_{\text{socL}}(\mathbf{k}) = \begin{pmatrix} 0 & 2 \cos \frac{k_y}{2} & -4i\lambda_{\text{soc}} \sin \frac{k_x}{2} \sin \frac{k_y}{2} \\ 2 \cos \frac{k_y}{2} & 0 & 2 \cos \frac{k_x}{2} \\ 4i\lambda_{\text{soc}} \sin \frac{k_x}{2} \sin \frac{k_y}{2} & 2 \cos \frac{k_x}{2} & 0 \end{pmatrix}, \quad (13)$$

where λ_{soc} denotes the strength of spin-orbit coupling. The flat band's energy is zero, i.e., $\varepsilon_{\text{socL},\text{fb}}(\mathbf{k}) = 0$, and the energies of the other two bands are

$$\varepsilon_{\text{socL},\pm}(\mathbf{k}) = \pm 2 \sqrt{\cos^2 \frac{k_x}{2} + \cos^2 \frac{k_y}{2} + 4\lambda_{\text{soc}}^2 \sin^2 \frac{k_x}{2} \sin^2 \frac{k_y}{2}}, \quad (14)$$

which are plotted in Fig. 2b for $\lambda_{\text{soc}} = 0.2$. The band gap between the IFB and its neighboring bands is given by $4|\lambda_{\text{soc}}|$ if $|\lambda_{\text{soc}}| < 1/2$, and 2 if $|\lambda_{\text{soc}}| \geq 1/2$, thus the flat band is decoupled from other bands for non-zero λ_{soc} .

The analytic form of the fidelity tensor $\chi_{xy}^{nm}(\mathbf{k})$ is given by

$$\chi_{\text{socL},xy}^{\text{fb},+}(\mathbf{k}) = \left(\chi_{\text{socL},xy}^{\text{fb},-}(\mathbf{k}) \right)^* = \frac{f(k_x, k_y) f(k_y, k_x)}{(\varepsilon_{\text{socL},+}(\mathbf{k}))^4 (2 + \cos k_x + \cos k_y)}, \quad (15)$$

where $f(k_x, k_y) = 4\lambda_{\text{soc}} \sin \frac{k_x}{2} \cos \frac{k_y}{2} (\cos^2 \frac{k_x}{2} + 1) + i\varepsilon_{\text{socL},+}(\mathbf{k}) \cos \frac{k_x}{2} \sin \frac{k_y}{2}$. Then, from Eq. (5), the modified band dispersion for the flat band is given by

$$E_{\text{fb},B}^{\text{socL}}(\mathbf{k}) = -\frac{2\pi\lambda_{\text{soc}}(3 - \cos k_x - \cos k_y - \cos k_x \cos k_y)}{(\varepsilon_{\text{socL},+}(\mathbf{k}))^2} \frac{\phi}{\phi_0}. \quad (16)$$

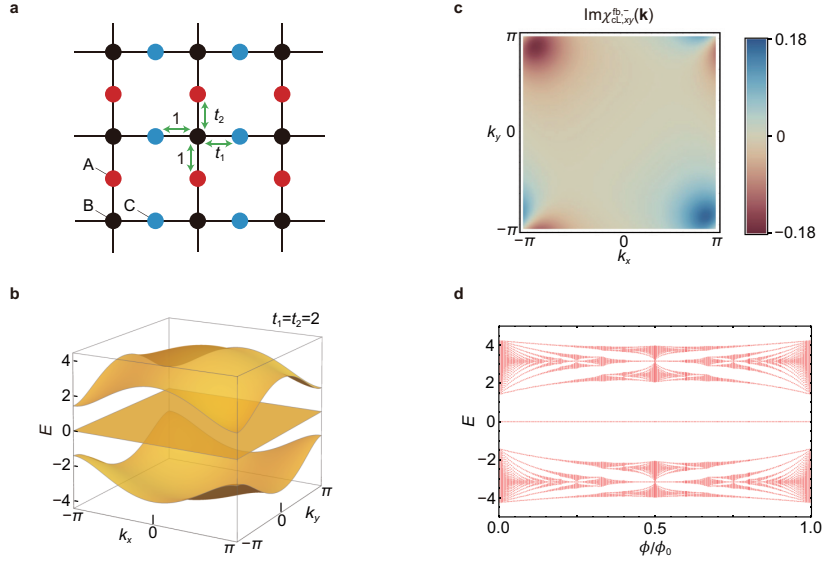


FIG. 3. **Landau level spreading of a flat-band system with chiral symmetry.** **a** Lattice structure for the c-Lieb model. The green arrows denote the hoppings. Note that the direction dependent hopping parameters induce a finite gap between the flat band and other bands. **b** The band structure for $H_{cL}(\mathbf{k})$ with $t_1 = t_2 = 2$. **c** Distribution of $\text{Im} \chi_{cL,xy}^{\text{fb},-}(\mathbf{k})$. Due to the chiral symmetry, $\text{Im} \chi_{cL,xy}^{\text{fb},-}(\mathbf{k}) = \text{Im} \chi_{cL,xy}^{\text{fb},+}(\mathbf{k})$ holds. **d** The Hofstadter spectrum of the c-Lieb model $H_{cL}(\mathbf{k})$ with $t_1 = t_2 = 2$. For any value of magnetic flux, the Landau levels of the flat band are fixed to the zero energy.

In Fig. 2c and d, $\text{Im} \chi_{\text{socL},xy}^{\text{fb},-}(\mathbf{k})$ and $E_{\text{fb},B}^{\text{socL}}(\mathbf{k})$ are shown. We note that

$$\max E_{\text{fb},B}^{\text{socL}}(\mathbf{k}) = E_{\text{fb},B}^{\text{socL}}(0, 0) = 0, \quad (17)$$

$$\min E_{\text{fb},B}^{\text{socL}}(\mathbf{k}) = \begin{cases} E_{\text{fb},B}^{\text{socL}}(\pi, \pi) = -\frac{\pi}{2\lambda_{\text{soc}}} \frac{\phi}{\phi_0} & (\lambda_{\text{soc}} \leq \frac{1}{2}) \\ E_{\text{fb},B}^{\text{socL}}(0, \pi) = -2\pi\lambda_{\text{soc}} \frac{\phi}{\phi_0} & (\lambda_{\text{soc}} > \frac{1}{2}) \end{cases}. \quad (18)$$

These minimum and maximum values of $E_{\text{fb},B}^{\text{socL}}(\mathbf{k})$ correspond to the lower and upper bounds for the LLS of the IFB as illustrated by red lines in Fig. 2e and f. Interestingly, the fidelity tensors $\chi_{\text{socL},xy}^{\text{fb},+}(\mathbf{k})$ and $\chi_{\text{socL},xy}^{\text{fb},-}(\mathbf{k})$ are conjugate of each other. This originates from the anti-unitary symmetry $C \circ I_{ST}$, a combination of chiral C and space-time-inversion I_{ST} symmetries, present in the system (see Supplementary Note 2 for the details.)

E. Chiral-symmetric system

We construct a chiral-symmetric Lieb (c-Lieb) model as a representative example for chiral-symmetric IFB systems. The c-Lieb is defined on the same Lieb lattice as the SOC-Lieb model, but with different hoppings. As shown in Fig. 3a, this model consists only of the nearest neighbor hoppings, denoted by green arrows. The hopping parameter from a B-site to a C-site is t_1 for the rightward hopping, and 1 for the leftward hopping. On the other hand, the hopping parameter from a B-site to an A-site is t_2 for the upward hopping, and 1 for the downward hopping. The corresponding tight-binding Hamiltonian in momentum space is given by

$$H_{cL}(\mathbf{k}) = \begin{pmatrix} 0 & e^{i\frac{k_y}{2}} + t_2 e^{-i\frac{k_y}{2}} & 0 \\ e^{-i\frac{k_y}{2}} + t_2 e^{i\frac{k_y}{2}} & 0 & e^{-i\frac{k_x}{2}} + t_1 e^{i\frac{k_x}{2}} \\ 0 & e^{i\frac{k_x}{2}} + t_1 e^{-i\frac{k_x}{2}} & 0 \end{pmatrix}, \quad (19)$$

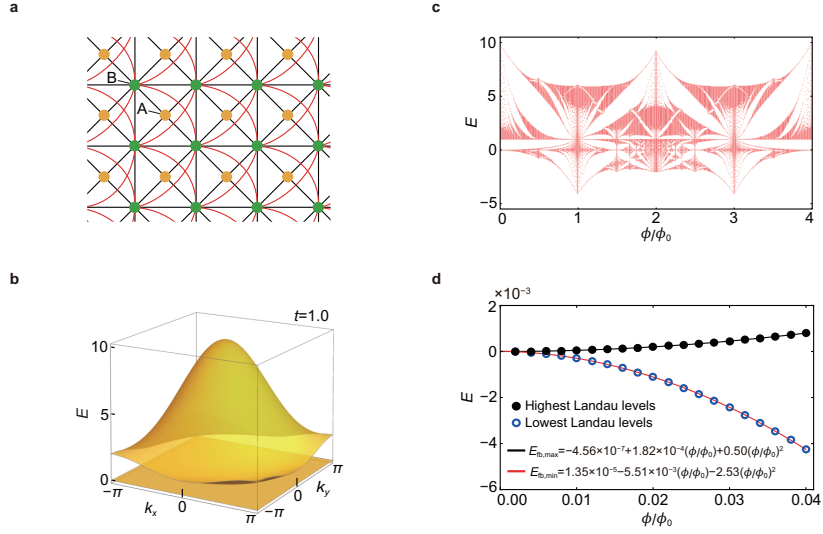


FIG. 4. **Landau level spreading of a flat-band system with space-time-inversion symmetry.** **a** The lattice structure for the I_{ST} -symmetric checkerboard model. The red and black lines denote the hopping processes between A and B sublattices. **b** The band structure of $H_{I_{ST}}(\mathbf{k})$ with $t = 1.0$. **c** The Hofstadter spectrum of the I_{ST} -symmetric checkerboard model with $t = 1.0$. **d** Variation of the lowest and highest Landau levels related to the flat band in the weak magnetic field (blue and black circles). $E_{fb,\min}(\phi/\phi_0)$ and $E_{fb,\max}(\phi/\phi_0)$ indicate the corresponding fitting functions (red and black solid lines) that exhibit quadratic magnetic field dependence dominantly.

with energy eigenvalues $\varepsilon_{cL,fb}(\mathbf{k}) = 0$ and $\varepsilon_{cL,\pm}(\mathbf{k}) = \pm\sqrt{2 + t_1^2 + t_2^2 + 2t_1 \cos k_x + 2t_2 \cos k_y}$. The chiral symmetry operator C is given by $C = \text{Diag}(1, -1, 1)$ which gives a symmetry relation,

$$CH_{cL}(\mathbf{k})C^{-1} = -H_{cL}(\mathbf{k}). \quad (20)$$

Note that the wave function of the flat band is also a simultaneous eigenstate of the chiral symmetry having a definite chiral charge $c = +1$:

$$C|u_{cL,fb}(\mathbf{k})\rangle = c|u_{cL,fb}(\mathbf{k})\rangle. \quad (21)$$

Also, we obtain the fidelity tensor $\chi_{xy}^{fb,\pm}$, expressed by

$$\chi_{cL,xy}^{fb,+}(\mathbf{k}) = \chi_{cL,xy}^{fb,-}(\mathbf{k}) = -\frac{(1 + t_1 e^{ik_x})(1 - t_1 e^{-ik_x})(1 + t_2 e^{-ik_y})(1 - t_2 e^{ik_y})}{8(\varepsilon_{cL,+}(\mathbf{k}))^4}. \quad (22)$$

The band structure and $\text{Im} \chi_{cL,xy}^{fb,-}(\mathbf{k})$ are shown in Fig. 3b and c. Equation (22) indicates that the modified band dispersion $E_{fb,B}(\mathbf{k})$ vanishes for all \mathbf{k} because $\varepsilon_{cL,+}(\mathbf{k}) = -\varepsilon_{cL,-}(\mathbf{k})$, which means that there is no LLS in the weak magnetic field. Also, we calculate the Hofstadter spectrum [29] for the c-Lieb model. Interestingly, we find that the LLS is absent even in the strong magnetic field, as shown in Fig. 3d. The existence of such zero-energy flat bands in the finite magnetic flux is guaranteed by chiral symmetry C . As explained in Supplementary Note 3, the minimal number of zero-energy flat bands is given by $|\text{Tr}[C]|$ at the zero magnetic flux. Moreover, when the system has the $|\text{Tr}[C]| (> 0)$ number of zero-energy flat bands at the zero magnetic flux, the LLS of flat band(s) is forbidden unless a gap closes at zero energy $E = 0$ as the magnetic flux increases (see Supplementary Note 3). In the c-Lieb model, such a gap closing at $E = 0$ does not occur at any magnetic flux. Hence, there is no LLS in all range of magnetic flux. On the other hand, when a gap closes at $E = 0$ as the magnetic flux increases, the LLS is forbidden only in a finite range of magnetic flux. As an example, in Supplementary Note 4, we show the Hofstadter spectrum of the ten-band model for twisted-bilayer graphene proposed in Ref. 30.

F. Space-time-inversion-symmetric system

The LLS of an IFB is weakly dependent on magnetic field when the system respects space-time-inversion I_{ST} symmetry at zero magnetic field. We consider spinless fermions on the checkerboard lattice shown in Fig. 4a, which is sometimes called

the Tasaki or decorated square lattice [31–33]. This model respects both time-reversal T and inversion I symmetries. Hence, a combined symmetry, space-time-inversion symmetry $I_{ST} = I \circ T$, exists. We note that the following discussion holds even if T and I are broken as long as I_{ST} is not broken. The tight-binding Hamiltonian consists of the hopping processes up to the third nearest neighbor hopping. In momentum space, the Hamiltonian is written as

$$H_{I_{ST}}(\mathbf{k}) = \begin{pmatrix} 1 & \cos \frac{k_+}{2} + 2t \cos \frac{k_-}{2} \\ \cos \frac{k_+}{2} + 2t \cos \frac{k_-}{2} & 2t \cos k_x + 2t \cos k_y + \cos^2 \frac{k_+}{2} + 4t^2 \cos^2 \frac{k_-}{2} \end{pmatrix}, \quad (23)$$

$$= \begin{pmatrix} 1 & \\ \cos \frac{k_+}{2} + 2t \cos \frac{k_-}{2} & \end{pmatrix} \left(1 \cos \frac{k_+}{2} + 2t \cos \frac{k_-}{2} \right), \quad (24)$$

where $k_{\pm} = k_x \pm k_y$. For $t = 1.0$, the band structure is shown in Fig. 4b. This system hosts a flat band with zero energy and a dispersive band with positive energy. The energy eigenvalues are given by $\varepsilon_{I_{ST},\uparrow}(\mathbf{k}) = 1 + (\cos \frac{k_+}{2} + 2t \cos \frac{k_-}{2})^2$ and $\varepsilon_{I_{ST},\text{fb}}(\mathbf{k}) = 0$.

In this system, I_{ST} is simply given by the complex conjugation, i.e., $I_{ST} = \mathcal{K}$ and

$$I_{ST}|u_{I_{ST},\text{fb}/\uparrow}(\mathbf{k})\rangle = |u_{I_{ST},\text{fb}/\uparrow}(\mathbf{k})\rangle. \quad (25)$$

Also, explicit calculations show $\text{Im} \chi_{I_{ST},xy}^{\text{fb},\uparrow}(\mathbf{k}) = 0$ and the vanishing modified band dispersion for the flat band $E_{n,B}(\mathbf{k}) = 0$, which results from Eq. (25). In Supplementary Note 2, we have proved that space-time inversion I_{ST} imposes $E_{n,B}(\mathbf{k}) = 0$ in general. We also note that $E_{n,B}(\mathbf{k}) = 0$ is consistent with the fact that the orbital angular momentum, which is proportional to the orbital magnetic moment, is constrained to be zero in I_{ST} -symmetric systems. Although the LLS is negligible in the weak magnetic field, it becomes considerably large in the strong magnetic field as shown in the Hofstadter spectrum in Fig. 4c. As shown in Fig. 4c, the Landau levels of the flat band acquire or lose their energy as the magnetic flux increases from 0 to some finite value much less than 1. This implies that the higher-order corrections of the magnetic field must be considered. Although it is out of the scope of this work, we present a fitting of the highest and lowest Landau levels of the flat band with respect to the magnetic flux:

$$E_{\text{fb},\text{min}}(\phi/\phi_0) = 1.35 \times 10^{-5} - 5.51 \times 10^{-3}(\phi/\phi_0) - 2.53(\phi/\phi_0)^2, \quad (26)$$

$$E_{\text{fb},\text{max}}(\phi/\phi_0) = -4.56 \times 10^{-7} + 1.82 \times 10^{-4}(\phi/\phi_0) + 0.50(\phi/\phi_0)^2, \quad (27)$$

which is plotted in Fig. 4d where one can observe the dominant quadratic dependence on the magnetic field.

Finally, we comment on the gap closing at $(\phi/\phi_0, E) = (1, 1.0)$ in the Hofstadter spectrum in Fig. 4c. At $(\phi/\phi_0, E) = (1, 1.0)$, the Landau levels related to the flat and dispersive bands show a closing of an indirect gap. We note that there is no closing of direct gaps in the Hofstadter Hamiltonian. Unlike the inevitable closing of the direct gap between topological bands in the finite magnetic flux reported before [11, 34], it is not necessary to close a direct gap in our system.

III. DISCUSSION

We have shown that the LLS of an IFB is determined by its wave-function geometry and the underlying symmetry of the system. The idea presented in this work goes beyond the conventional semiclassical idea in which the Landau level spectrum is dominantly determined by the band dispersion at zero magnetic field. So far, we have focused on the cases when the band width of the IFB is strictly zero. However, in real materials, it is difficult to observe perfect flat bands due to the long-range hoppings and spin-orbit coupling [35–39]. To understand the influence of a finite band width of the IFB, we have studied another tight-binding model defined in the Lieb lattice including spin-orbit coupling. The hopping parameters, the band structure, and the LLS of this system are described in Fig. 2a, Fig. 5a, and Fig. 5b,c, respectively. Under weak magnetic flux with $t\lambda_{\text{soc}}\phi > 0$, the LLS of the IFB cannot be observed because it is dominated by the energy scale of the band width of the nearly flat band. However, the anomalous LLS arising from the wave-function ge-

ometry can be observed for the magnetic flux larger than a threshold value $(\phi/\phi_0)_{\text{thres}} \sim 8t\lambda_{\text{soc}}/\pi$ (see Fig. 5c). On the other hand, the LLS is not disturbed by the band width when $t\lambda_{\text{soc}}\phi < 0$, because the nearly flat band has only positive energy (see Fig. 5c). Such a Lieb lattice model with spin-orbit coupling hosting a nearly flat band was already realized in an exciton-polariton system [40], and also is expected to be realized in electronic systems consisting of covalently-bonded organic frameworks [41].

Finally, we discuss the influence of disorder on the LLS of an IFB and the related Landau level fan diagram. The fan diagram is obtained by calculating the density of states (DOS) of Landau levels of the disordered SOC Lieb model including a random impurity potential whose maximum strength is denoted by W (see Methods for details). As shown in Fig. 5d and e, aside from the huge and wide DOS peaks from the dense Landau levels with higher Landau level indices, one can find small but sharp peaks corresponding to the LLLs of the IFB, from which the LLS of the IFB can be determined. While this LLL peak is buried in the DOS

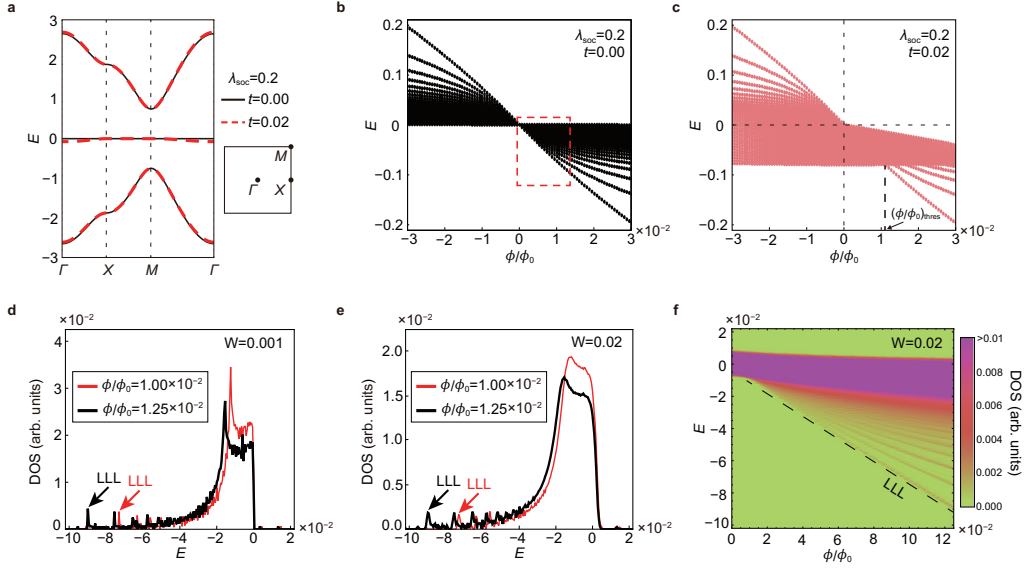


FIG. 5. **Influence of finite band width and disorder on the Landau level spreading of IFBs.** **a-c** A nearly-flat band in the spin-orbit coupled Lieb lattice where the dispersion of the FB arises from the next nearest neighbor hoppings between A and C sublattices with the amplitude t (see Fig. 2a). **a** The band structure of the nearly-flat-Lieb model with $(t, \lambda_{\text{soc}}) = (0, 0.2)$ and $(0.02, 0.2)$, which are denoted by the black and red lines, respectively. The right side of the band structure describes the first Brillouin zone and the high-symmetry points. **b** The Landau levels in the weak magnetic field for $t = 0.00$ and $\lambda_{\text{soc}} = 0.2$. The lowest (highest) Landau level has the energy $-\frac{\pi}{2\lambda_{\text{soc}}}\phi/\phi_0$ when $\phi > 0$ ($\phi < 0$). **c** Similar plot for $t = 0.02$ and $\lambda_{\text{soc}} = 0.2$. When $\phi > 0$, the LLS can be observed once the magnetic flux exceeds the threshold value $(\phi/\phi_0)_{\text{thres}} \sim \frac{8t\lambda_{\text{soc}}}{\pi}$ because of the finite band width $4t$. While, the threshold magnetic flux is zero when $\phi < 0$ since the LLS develops only in the negative energy direction. **d-f** Density of states (DOS) of Landau levels in the presence of disorder. **d** DOS of Landau levels in very clean system with $W = 0.001$. The red (black) line corresponds to $\phi/\phi_0 = 1.00 \times 10^{-2}$ (1.25×10^{-2}). The lowest Landau level (LLL) peaks are denoted by black and red arrows. The energy range of the plot corresponds to the red dashed box in **(b)**. **e** DOS of Landau levels for $W = 0.02$. **f** The intensity plot of the DOS (or the Landau fan diagram) for $W = 0.02$ and the iteration number $N_{\text{itr}} = 20$ as a function of ϕ/ϕ_0 . The plot ranges for the energy and magnetic flux correspond to the red dashed box in **(b)**. The black dashed line indicates the LLL peak positions. Note that the maximum value of DOS in the plotted region is 2.306×10^{-2} (arb. unit).

envelope of the higher Landau levels in the weak magnetic field, it splits away from this envelope as the magnetic field is large enough as shown in Fig. 5f. From the fan diagram, one can check the geometric principle described by Eq. (5) by extracting the slope of the LLL, which is represented by the dashed guide line in Fig. 5f. Here we considered the magnetic fluxes ϕ/ϕ_0 below 1.25×10^{-2} , which correspond to the experimentally accessible region. Note that when the size of a unit cell is equal to $l\text{nm}$, the relevant magnetic field is about $B \sim 4000 \times \phi/\phi_0 \times l^{-2}(\text{T})$ approximately. For instance, in the case of the Lieb lattice composed of the covalently-bonded organic frameworks [41], $\phi/\phi_0 = 1.25 \times 10^{-2}$ corresponds to $B \sim 50T$. We expect the DOS peak corresponding to the LLL to be detected by the resistance measurement from magnetotransport experiments or the dI/dV measurement from the scanning tunneling spectroscopy if the magnetic field is strong enough or the system is sufficiently clean so that the Landau level spacing becomes larger than the Landau level broadening. Especially, when the LLS develops asymmetrically, like in Fig. 5b, an overall energy shift of the DOS from the flat band's energy appears more prominently, which provides a direct experimental signature of the LLS even in disordered systems.

Up to now, our discussion has been focused on con-

ventional materials to realize flat bands. However, it is worth noting that there are various artificial systems such as photonic systems [13, 42–44], optical lattices [45–50], and systems with synthetic dimensions [51–55], which could offer better opportunities to test our theoretical prediction. In these systems, the band engineering is relatively easier, and controlled experiments with artificial magnetic fields can also be performed. Designing realistic experimental setups for observing LLS of flat bands in such artificial systems would be one important problem for future study.

METHODS

A. Symmetry constraints on the LLS

In order to derive the symmetry constraints on $E_{n,B}(\mathbf{k})$ and $\chi_{xy}^{nm}(\mathbf{k})$, let us consider a symmetry operation σ acting on the Hamiltonian,

$$U_\sigma(\mathbf{k})\overline{H(\mathbf{k})}^s U_\sigma(\mathbf{k})^\dagger = pH(O_\sigma\mathbf{k}), \quad (28)$$

where $s \in \{0, 1\}$, $p \in \{-1, 1\}$, U_σ indicates a unitary matrix representing the symmetry σ , and $\bar{x} = x^*$ means the complex conjugation of x . From now on, we use a compact notation $\mathbf{g}_\sigma = (O_\sigma, s, p)$ to describe the operation of the symmetry σ . For example, $\mathbf{g}_T = (-\mathbb{1}_d, 1, 1)$ is used for time-reversal symmetry T where d and $\mathbb{1}_d$ denote the dimensionality and the $d \times d$ identity matrix, respectively. The symmetry constraints on $E_{n,B}(\mathbf{k})$ and $\chi_{ij}^{nm}(\mathbf{k})$ derived from Eq. (28) are

$$E_{n,B}(O_\sigma \mathbf{k}) = (-1)^s p \text{Det} O_\sigma E_{n,B}(\mathbf{k}), \quad (29)$$

$$\chi_{ij}^{nm\sigma}(O_\sigma \mathbf{k}) = [O_\sigma]_{ii'} [O_\sigma]_{jj'} \overline{\chi_{i'j'}^{nm}(\mathbf{k})}^s, \quad (30)$$

where the band indices m and m_σ in Eq. (30) are chosen such that $\varepsilon_m(\mathbf{k}) = p \varepsilon_{m_\sigma}(O_\sigma \mathbf{k})$. Detailed derivation of Eqs. (29) and (30) and comments on the degenerate bands can be found in Supplementary Note 2. From Eq. (29), we obtain two symmetries that give vanishing modified band dispersion, $E_{n,B}(\mathbf{k}) = 0$: $\mathbf{g}_C = (\mathbb{1}_d, 0, -1)$ and $\mathbf{g}_{I_{ST}} = (\mathbb{1}_d, 1, 1)$ which correspond to chiral symmetry C and space-time-inversion symmetry I_{ST} , respectively. On the other hand, when $(-1)^s p \text{Det} O_\sigma = -1$ and $\text{Det} O_\sigma \neq 1$, the modified band dispersion satisfies $E_{n,B}(O_\sigma \mathbf{k}) = -E_{n,B}(\mathbf{k})$, which implies $\max E_{n,B}(\mathbf{k}) = -\min E_{n,B}(\mathbf{k})$. Time-reversal T and reflection R symmetries belong to this case. Also, the contribution to the $E_{n,B}(\mathbf{k})$ from each band via the inter-band coupling in Eq. (5) can be systematically understood by using Eq. (30) (see Supplementary Note 2 for details).

B. Calculation scheme for the Landau levels

We calculate the Hofstadter spectrum by numerically implementing the Peierls substitution to the tight-binding Hamiltonian [29].

C. Calculation of Landau fan diagram including disorder

To obtain the Landau fan diagram including disorder effect, we study a finite-size SOC Lieb model $H_{\text{socL}}(\mathbf{k})$ composed of 40 by 40 unit cells. Disorder is introduced by the Hamiltonian H_{dis} with components $(H_{\text{dis}})_{ij} = w_i \delta_{ij}$, where $i, j = 1, \dots, 4800$ denotes the unit cell index and $w_i \in [-W/2, W/2]$ follows a uniform probability distribution. By diagonalizing the disordered Hamiltonian $N_{\text{itr}} = 200$ times and averaging the results, the density of states (DOS) of Landau levels is obtained. Note that chiral edge states are found in the gap between flat and dispersive bands. It is because the two dispersive bands in the SOC Lieb model have the Chern number ± 1 respectively depending on the sign of spin-orbit coupling, despite the topologically trivial middle flat band. However, the contribution of edge states to DOS is quantitatively negligible.

Data availability The data that support the findings of this study are available from the corresponding authors upon reasonable request.

Code availability The numerical codes used in this paper are available from the corresponding authors upon reasonable request.

ACKNOWLEDGMENTS

Y.H. was supported by IBS-R009-D1 and Samsung Science and Technology Foundation under Project Number SSTF-BA2002-06. J.W.R. was supported by IBS-R009-D1, and the National Research Foundation of Korea (NRF) Grant funded by the Korea government (MSIT) (Grant No. 2021R1A2C1010572). B.J.Y. was supported by the Institute for Basic Science in Korea (Grant No. IBS-R009-D1), Samsung Science and Technology Foundation under Project Number SSTF-BA2002-06, the National Research Foundation of Korea (NRF) Grant funded by the Korea government (MSIT) (No.2021R1A2C4002773, and No. NRF-2021R1A5A1032996), and the U.S. Army Research Office and Asian Office of Aerospace Research & Development (AOARD) under Grant No. W911NF-18-1-0137.

Author contributions Y.H. and J.W.R. performed theoretical and numerical analyses. B.J.Y. supervised the project. All authors analysed the data. The manuscript was written by all authors.

Competing interests The authors declare no competing interests.

Correspondence and requests for materials should be addressed to J.-W. R. or B.-J. Y.

REFERENCES

- [1] L. Onsager, The London, Edinburgh, and Dublin Philosophical Magazine and Journal of Science **43**, 1006 (1952).
- [2] L. M. Roth, Physical Review **145**, 434 (1966).
- [3] G. Mikitik and Y. V. Sharlai, Physical Review Letters **82**, 2147 (1999).
- [4] Y. Gao and Q. Niu, Proceedings of the National Academy of Sciences **114**, 7295 (2017).
- [5] J.-N. Fuchs, F. Piéchon, and G. Montambaux, SciPost Physics **4**, 024 (2018).
- [6] Y. Zhang, Y.-W. Tan, H. L. Stormer, and P. Kim, Nature **438**, 201 (2005).
- [7] K. S. Novoselov, E. McCann, S. Morozov, V. I. Fal'ko, M. Katshnelson, U. Zeitler, D. Jiang, F. Schedin, and A. Geim, Nature Physics **2**, 177 (2006).
- [8] M.-C. Chang and Q. Niu, Physical Review B **53**, 7010 (1996).
- [9] H. C. Po, H. Watanabe, and A. Vishwanath, Physical Review Letters **121**, 126402 (2018).
- [10] J. Ahn, S. Park, and B.-J. Yang, Physical Review X **9**, 021013 (2019).
- [11] B. Lian, F. Xie, and B. A. Bernevig, Physical Review B **102**, 041402(R) (2020).
- [12] J.-W. Rhim and B.-J. Yang, Physical Review B **99**, 045107 (2019).

- [13] J. Ma, J.-W. Rhim, L. Tang, S. Xia, H. Wang, X. Zheng, S. Xia, D. Song, Y. Hu, Y. Li, *et al.*, *Physical Review Letters* **124**, 183901 (2020).
- [14] J.-W. Rhim, K. Kim, and B.-J. Yang, *Nature* **584**, 59 (2020).
- [15] L. Chen, T. Mazaheri, A. Seidel, and X. Tang, *Journal of Physics A: Mathematical and Theoretical* **47**, 152001 (2014).
- [16] N. Read, *Physical Review B* **95**, 115309 (2017).
- [17] A. Alexandradinata and J. Höller, *Physical Review B* **98**, 184305 (2018).
- [18] D.-S. Ma, Y. Xu, C. Chiu, N. Regnault, A. Houck, Z. Song, and B. Bernevig, *Physical Review Letters* **125**, 266403 (2020).
- [19] C. Chiu, D.-S. Ma, Z.-D. Song, B. Bernevig, and A. Houck, *Physical Review Research* **2**, 043414 (2020).
- [20] F. de Juan, A. G. Grushin, T. Morimoto, and J. E. Moore, *Nature Communications* **8**, 15995 (2017).
- [21] V. Bužek and M. Hillery, *Physical Review A* **54**, 1844 (1996).
- [22] V. Dodonov, O. Man'Ko, V. Man'Ko, and A. Wünsche, *Journal of Modern Optics* **47**, 633 (2000).
- [23] M. V. Berry, *Geometric phases in physics*, 7 (1989).
- [24] J. Provost and G. Vallee, *Communications in Mathematical Physics* **76**, 289 (1980).
- [25] P. Zanardi, P. Giorda, and M. Cozzini, *Physical Review Letters* **99**, 100603 (2007).
- [26] Y.-Q. Ma, S. Chen, H. Fan, W.-M. Liu, *et al.*, *Physical Review B* **81**, 245129 (2010).
- [27] R. Jozsa, *Journal of modern optics* **41**, 2315 (1994).
- [28] N. Goldman, D. Urban, and D. Bercioux, *Physical Review A* **83**, 063601 (2011).
- [29] D. R. Hofstadter, *Physical Review B* **14**, 2239 (1976).
- [30] H. C. Po, L. Zou, T. Senthil, and A. Vishwanath, *Physical Review B* **99**, 195455 (2019).
- [31] H. Tasaki, *Physical Review Letters* **69**, 1608 (1992).
- [32] H. Aoki, M. Ando, and H. Matsumura, *Physical Review B* **54**, R17296 (1996).
- [33] T. Misumi and H. Aoki, *Physical Review B* **96**, 155137 (2017).
- [34] J. Herzog-Arbeitman, Z.-D. Song, N. Regnault, and B. A. Bernevig, *Physical Review Letters* **125**, 236804 (2020).
- [35] S. Taie, H. Ozawa, T. Ichinose, T. Nishio, S. Nakajima, and Y. Takahashi, *Science Advances* **1**, e1500854 (2015).
- [36] S. Kajiwara, Y. Urade, Y. Nakata, T. Nakanishi, and M. Kitano, *Physical Review B* **93**, 075126 (2016).
- [37] M. R. Slot, T. S. Gardenier, P. H. Jacobse, G. C. van Miert, S. N. Kempkes, S. J. Zevenhuizen, C. M. Smith, D. Vanmaekelbergh, and I. Swart, *Nature Physics* **13**, 672 (2017).
- [38] R. Drost, T. Ojanen, A. Harju, and P. Liljeroth, *Nature Physics* **13**, 668 (2017).
- [39] D. Leykam, A. Andreanov, and S. Flach, *Advances in Physics: X* **3**, 1473052 (2018).
- [40] C. Whittaker, E. Cancellieri, P. Walker, D. Gulevich, H. Schomerus, D. Vaitiekus, B. Royall, D. Whittaker, E. Clarke, I. Iorsh, *et al.*, *Physical Review Letters* **120**, 097401 (2018).
- [41] B. Cui, X. Zheng, J. Wang, D. Liu, S. Xie, and B. Huang, *Nature Communications* **11**, 66 (2020).
- [42] R. A. Vicencio, C. Cantillano, L. Morales-Inostroza, B. Real, C. Mejía-Cortés, S. Weimann, A. Szameit, and M. I. Molina, *Physical Review Letters* **114**, 245503 (2015).
- [43] F. Baboux, L. Ge, T. Jacqmin, M. Biondi, E. Galopin, A. Lemaître, L. Le Gratiet, I. Sagnes, S. Schmidt, H. Türeci, *et al.*, *Physical Review Letters* **116**, 066402 (2016).
- [44] T. Ozawa, H. M. Price, A. Amo, N. Goldman, M. Hafezi, L. Lu, M. C. Rechtsman, D. Schuster, J. Simon, O. Zilberberg, *et al.*, *Reviews of Modern Physics* **91**, 015006 (2019).
- [45] I. Bloch, *Nature Physics* **1**, 23 (2005).
- [46] M. Aidelsburger, M. Atala, S. Nascimbene, S. Trotzky, Y.-A. Chen, and I. Bloch, *Physical Review Letters* **107**, 255301 (2011).
- [47] C. Wu, D. Bergman, L. Balents, and S. D. Sarma, *Physical Review Letters* **99**, 070401 (2007).
- [48] V. Apaja, M. Hyrkäs, and M. Manninen, *Physical Review A* **82**, 041402 (2010).
- [49] B. Song, C. He, S. Niu, L. Zhang, Z. Ren, X.-J. Liu, and G.-B. Jo, *Nature Physics* **15**, 911 (2019).
- [50] B. Tian, M. Endres, and D. Pekker, *Physical Review Letters* **115**, 236803 (2015).
- [51] T. Ozawa and H. M. Price, *Nature Reviews Physics* **1**, 349 (2019).
- [52] A. Celi, P. Massignan, J. Ruseckas, N. Goldman, I. B. Spielman, G. Juzeliūnas, and M. Lewenstein, *Physical Review Letters* **112**, 043001 (2014).
- [53] T. Ozawa and I. Carusotto, *Physical Review Letters* **118**, 013601 (2017).
- [54] T. Ozawa, *Physical Review A* **103**, 033318 (2021).
- [55] A. Dutt, M. Minkov, Q. Lin, L. Yuan, D. A. Miller, and S. Fan, *Nature Communications* **10**, 3122 (2019).
- [56] G. Sundaram and Q. Niu, *Physical Review B* **59**, 14915 (1999).
- [57] Z. Song, Z. Wang, W. Shi, G. Li, C. Fang, and B. A. Bernevig, *Physical Review Letters* **123**, 036401 (2019).

Supplementary Information for “Geometric characterization of anomalous Landau levels of isolated flat bands”

Supplementary Note 1. Derivation of the relation between the Landau level spreading of an isolated flat band and cross-gap Berry connection

In the main text, the Landau level spreading of an isolated flat band is related to the cross-gap Berry connection and fidelity tensor through Eq. (5) of the main text. In this Supplementary Note, we derive Eq. (5) of the main text from the definition of the modified band structure $E_{n,B}(\mathbf{k})$ and the orbital magnetic moment $\mu_n(\mathbf{k})$, which are given by Eqs. (3) and (4) of the main text respectively. Recall that the modified band structure of n th band is expressed as

$$E_{n,B}(\mathbf{k}) = \varepsilon_n(\mathbf{k}) + \mu_n(\mathbf{k})B, \quad (\text{S1})$$

where $\varepsilon_n(\mathbf{k})$ denotes band dispersion of n th band in the zero magnetic field. The orbital magnetic moment $\mu_n(\mathbf{k})$ arises from the self rotation of wave packet corresponding to n th band, and it is given by

$$\mu_n(\mathbf{k}) = \frac{e}{\hbar} \text{Im} \langle \partial_x u_n(\mathbf{k}) | [\varepsilon_n(\mathbf{k}) - H(\mathbf{k})] | \partial_y u_n(\mathbf{k}) \rangle, \quad (\text{S2})$$

where $\partial_i = \partial_{k_i}$ ($i = x, y$) and $|u_n(\mathbf{k})\rangle$ denotes the periodic part of Bloch wave function of n th band. These results, Eqs. (S1) and (S2), were obtained by M.-C. Chang and Q. Niu [8].

Before deriving Eq. (5) of the main text, we review how Eqs. (3) and (4) of the main text can be obtained from the semiclassical theory of wave packet dynamics by closely following Refs. 8 and 56. First, let us consider a periodic Hamiltonian $H_0(\hat{\mathbf{r}}, \hat{\mathbf{p}})$ and the Bloch wave function $|\psi_n(\mathbf{q})\rangle$ for n th band such that $H_0(\hat{\mathbf{r}}, \hat{\mathbf{p}})|\psi_n(\mathbf{q})\rangle = \varepsilon_n(\mathbf{q})|\psi_n(\mathbf{q})\rangle$ where \mathbf{q} is the crystal momentum. Correspondingly, the Bloch Hamiltonian, $H_{0\mathbf{q}}(\hat{\mathbf{r}}, \hat{\mathbf{p}}) = e^{-i\mathbf{q}\cdot\hat{\mathbf{r}}}H_0(\hat{\mathbf{r}}, \hat{\mathbf{p}})e^{i\mathbf{q}\cdot\hat{\mathbf{r}}}$, and the periodic part of Bloch wave function, $|u_n(\mathbf{q})\rangle = e^{i\mathbf{q}\cdot\hat{\mathbf{r}}}|\psi_n(\mathbf{q})\rangle$, satisfy a similar eigenvalue equation, $H_{0\mathbf{q}}(\hat{\mathbf{r}}, \hat{\mathbf{p}})|u_n(\mathbf{q})\rangle = \varepsilon_n(\mathbf{q})|u_n(\mathbf{q})\rangle$. From now on, we omit the argument of Hamiltonian unless there is no confusion.

In the presence of constant magnetic field, the vector potential can be chosen as $\mathbf{A}(\mathbf{r}) = \frac{1}{2}\mathbf{B} \times \mathbf{r}$. As the vector potential changes the Hamiltonian according to the Peierls substitution, the Hamiltonian in the magnetic field becomes $H = H_0(\hat{\mathbf{r}}, \hat{\mathbf{p}} + e\mathbf{A}(\hat{\mathbf{r}}))$. When a semiclassical wave packet is localized at \mathbf{r}_c in real space, one can consider the derivative expansion of H near \mathbf{r}_c . Up to first order in B , the Hamiltonian is divided into *unperturbed* Hamiltonian H_1 and *perturbation* Hamiltonian H_2 , i.e. $H = H_1 + H_2$. Explicitly, $H_{1,2}$ are expressed by

$$H_1 = H_0(\hat{\mathbf{r}}, \hat{\mathbf{p}} + e\mathbf{A}(\mathbf{r}_c)), \quad H_2 = \frac{e}{4m}\mathbf{B} \cdot [(\hat{\mathbf{r}} - \mathbf{r}_c) \times \hat{\mathbf{P}}] + h.c., \quad (\text{S3})$$

where $\hat{\mathbf{P}} = -i\frac{m}{\hbar}[\hat{\mathbf{r}}, H_1]$ is the momentum operator. H_1 is the Hamiltonian that the wave packet experiences at its center \mathbf{r}_c . H_2 is the coupling between the orbital magnetic moment and the magnetic field. This can be seen by noticing that $\mathbf{L} = \frac{1}{2}(\hat{\mathbf{r}} - \mathbf{r}_c) \times \hat{\mathbf{P}} - \frac{1}{2}\hat{\mathbf{P}} \times (\hat{\mathbf{r}} - \mathbf{r}_c)$ where \mathbf{L} is the angular momentum resulted from the self rotation of wave packet around its center. Hence, $H_2 = \frac{e}{2m}\mathbf{B} \cdot \mathbf{L} \simeq \mu \cdot \mathbf{B}$ where we define the orbital magnetic moment as $\mu \simeq \frac{e}{2m}\mathbf{L}$.

As we treat H_1 as the unperturbed Hamiltonian, the corresponding unperturbed eigenstates should be identified. Since $H_1 = H_0(\hat{\mathbf{r}}, \hat{\mathbf{p}} + e\mathbf{A}(\mathbf{r}_c)) = e^{-ie\mathbf{A}(\mathbf{r}_c)\cdot\hat{\mathbf{r}}}H_0(\hat{\mathbf{r}}, \hat{\mathbf{p}})e^{ie\mathbf{A}(\mathbf{r}_c)\cdot\hat{\mathbf{r}}}$, one can define $H_{1\mathbf{q}} = e^{-i\mathbf{q}\cdot\hat{\mathbf{r}}}H_1e^{i\mathbf{q}\cdot\hat{\mathbf{r}}} = e^{-i\mathbf{k}\cdot\hat{\mathbf{r}}}H_0e^{i\mathbf{k}\cdot\hat{\mathbf{r}}}$ by introducing the gauge-invariant crystal momentum $\mathbf{k} = \mathbf{q} + \frac{e}{\hbar}\mathbf{A}(\mathbf{r}_c)$. From $H_{1\mathbf{q}} = e^{-i\mathbf{k}\cdot\hat{\mathbf{r}}}H_0e^{i\mathbf{k}\cdot\hat{\mathbf{r}}}$, $H_{1\mathbf{q}}$ can also be identified as $H_{0\mathbf{k}}$. Hence, the Bloch wave function and its periodic part must be chosen such that $H_{0\mathbf{k}}|u_n(\mathbf{k})\rangle = \varepsilon_n(\mathbf{k})|u_n(\mathbf{k})\rangle$, $H_1|\psi_n(\mathbf{k})\rangle = \varepsilon_n(\mathbf{k})|\psi_n(\mathbf{k})\rangle$, and $|\psi_n(\mathbf{k})\rangle = e^{i\mathbf{q}\cdot\hat{\mathbf{r}}}|u_n(\mathbf{k})\rangle$. Once the unperturbed eigenstates are identified, a semiclassical wave packet $|W_n\rangle$ can be constructed as follows. $|W_n\rangle$ is a superposition of $|\psi_n(\mathbf{k})\rangle$ with different momenta \mathbf{k} : $|W_n\rangle = \sum_{\mathbf{q}} w(\mathbf{q})|\psi_n(\mathbf{k})\rangle = \sum_{\mathbf{q}} w(\mathbf{q})e^{i\mathbf{q}\cdot\hat{\mathbf{r}}}|u_n(\mathbf{k})\rangle$ where the amplitude $w(\mathbf{q})$ are normalized according to $\sum_{\mathbf{q}} \overline{w(\mathbf{q})}w(\mathbf{q}) = 1$. Since the wave packet is localized at real-space center \mathbf{r}_c and momentum-space center \mathbf{q}_c , the amplitude $w(\mathbf{q})$ must satisfy $\langle W_n | \hat{\mathbf{r}} | W_n \rangle = \mathbf{r}_c$ and $\overline{w(\mathbf{q})}w(\mathbf{q}) \simeq \delta_{\mathbf{q}, \mathbf{q}_c}$. Note that \bar{x} and δ denote the complex conjugation of x and the Kronecker delta symbol, respectively.

Now, we can calculate the energy expectation value $\langle W_n | H | W_n \rangle = E_1 + E_2$ where $E_{1,2} = \langle W_n | H_{1,2} | W_n \rangle$. First, E_1 can be obtained straightforwardly,

$$E_1 = \langle W_n | H_1 | W_n \rangle = \sum_{\mathbf{q}} \overline{w(\mathbf{q})}w(\mathbf{q})\varepsilon_n(\mathbf{k}) \simeq \varepsilon_n(\mathbf{k}_c), \quad (\text{S4})$$

where $\mathbf{k}_c = \mathbf{q}_c + \frac{e}{\hbar}\mathbf{A}(\mathbf{r}_c)$. Hence, E_1 is nothing but the unperturbed band dispersion at momentum \mathbf{k}_c . The energy correction

E_2 can be written as

$$\begin{aligned}
\langle W_n | H_2 | W_n \rangle &= \sum_{\mathbf{q}, \mathbf{q}'} \overline{w(\mathbf{q}')} w(\mathbf{q}) \langle \psi_n(\mathbf{k}') | H_2 | \psi_n(\mathbf{k}) \rangle \\
&= -i \frac{e}{4\hbar} \mathbf{B} \cdot \sum_{\mathbf{q}, \mathbf{q}'} \overline{w(\mathbf{q}')} w(\mathbf{q}) \langle u_n(\mathbf{k}') | (\hat{\mathbf{r}} - \mathbf{r}_c) \times e^{-i\mathbf{q}' \cdot \hat{\mathbf{r}}} [\hat{\mathbf{r}}, H_1] e^{i\mathbf{q} \cdot \hat{\mathbf{r}}} | u_n(\mathbf{k}) \rangle + h.c. \\
&= \frac{e}{4\hbar} \mathbf{B} \cdot \sum_{\mathbf{q}, \mathbf{q}'} \overline{w(\mathbf{q}')} w(\mathbf{q}) \langle u_n(\mathbf{k}') | (\hat{\mathbf{r}} - \mathbf{r}_c) e^{-i(\mathbf{q}' - \mathbf{q}) \cdot \hat{\mathbf{r}}} \times \partial_{\mathbf{k}} H_{0\mathbf{k}} | u_n(\mathbf{k}) \rangle + h.c., \\
&= \frac{e}{4\hbar} \mathbf{B} \cdot \sum_{\mathbf{q}, \mathbf{q}'} \overline{w(\mathbf{q}')} w(\mathbf{q}) \mathbf{F}(\mathbf{k}', \mathbf{k}) + h.c., \tag{S5}
\end{aligned}$$

where $[\hat{\mathbf{r}}, H_{0\mathbf{k}}] = i\partial_{\mathbf{k}} H_{0\mathbf{k}}$ is applied in the third equality and we define $\mathbf{F}(\mathbf{k}', \mathbf{k}) = \langle u_n(\mathbf{k}') | (\hat{\mathbf{r}} - \mathbf{r}_c) e^{-i(\mathbf{q}' - \mathbf{q}) \cdot \hat{\mathbf{r}}} \times \partial_{\mathbf{k}} H_{0\mathbf{k}} | u_n(\mathbf{k}) \rangle$ for notational simplicity. The expression for $F(\mathbf{k}', \mathbf{k})$ can be simplified with the help of various identities such as $\hat{\mathbf{r}} = i\partial_{\mathbf{q}} e^{-i\mathbf{q} \cdot \hat{\mathbf{r}}} e^{i\mathbf{q} \cdot \hat{\mathbf{r}}}$ and $\partial_{\mathbf{k}} H_{0\mathbf{k}} | u_n(\mathbf{k}) \rangle = \partial_{\mathbf{k}} \varepsilon_n(\mathbf{k}) | u_n(\mathbf{k}) \rangle + (\varepsilon_n(\mathbf{k}) - H_{0\mathbf{k}}) | \partial_{\mathbf{k}} u_n(\mathbf{k}) \rangle$. We also use $\langle f_1(\mathbf{q}') | e^{-i(\mathbf{q}' - \mathbf{q}) \cdot \hat{\mathbf{r}}} | f_2(\mathbf{q}) \rangle = \langle f_1(\mathbf{q}) | f_2(\mathbf{q}) \rangle \delta_{\mathbf{q}', \mathbf{q}}$, which holds for two states $|f_{1,2}(\mathbf{q})\rangle$ that are periodic in real space. Applying these identities, we obtain

$$\begin{aligned}
\mathbf{F}(\mathbf{k}', \mathbf{k}) &= i \langle u_n(\mathbf{k}') | \left[(\partial_{\mathbf{q}'} - \mathbf{r}_c) e^{-i(\mathbf{q}' - \mathbf{q}) \cdot \hat{\mathbf{r}}} \right] \times [\partial_{\mathbf{k}} \varepsilon_n(\mathbf{k}) | u_n(\mathbf{k}) \rangle + (\varepsilon_n(\mathbf{k}) - H_{0\mathbf{k}}) | \partial_{\mathbf{k}} u_n(\mathbf{k}) \rangle] \\
&= (i\partial_{\mathbf{k}'} \delta_{\mathbf{k}', \mathbf{k}} - \mathbf{r}_c + A_n(\mathbf{k})) \times \partial_{\mathbf{k}} \varepsilon_n(\mathbf{k}) - i \langle \partial_{\mathbf{k}} u_n(\mathbf{k}) | \times [\varepsilon_n(\mathbf{k}) - H_{0\mathbf{k}}] | \partial_{\mathbf{k}} u_n(\mathbf{k}) \rangle, \tag{S6}
\end{aligned}$$

where $A_n(\mathbf{k}) = -i \langle \partial_{\mathbf{k}} u_n(\mathbf{k}) | u_n(\mathbf{k}) \rangle$. Here, we treat the Kronecker delta as the Dirac delta function with the appropriate numerical factor. The substitution of Eq. (S6) into Eq. (S5) leads to

$$\begin{aligned}
E_2 &= -\frac{ie}{4\hbar} \mathbf{B} \cdot \sum_{\mathbf{q}} |w(\mathbf{q})|^2 \langle \partial_{\mathbf{k}} u_n(\mathbf{k}) | \times [\varepsilon_n(\mathbf{k}) - H_{0\mathbf{k}}] | \partial_{\mathbf{k}} u_n(\mathbf{k}) \rangle \\
&\quad + \frac{e}{4\hbar} \mathbf{B} \cdot \sum_{\mathbf{q}} \left[-iw(\mathbf{q}) \partial_{\mathbf{q}} \overline{w(\mathbf{q})} + (A_n(\mathbf{k}) - \mathbf{r}_c) |w(\mathbf{q})|^2 \right] \times \partial_{\mathbf{k}} \varepsilon_n(\mathbf{k}) + h.c. \\
&\simeq -\frac{ie}{4\hbar} \mathbf{B} \cdot \langle \partial_{\mathbf{k}_c} u_n(\mathbf{k}_c) | \times [\varepsilon_n(\mathbf{k}_c) - H_{0\mathbf{k}_c}] | \partial_{\mathbf{k}_c} u_n(\mathbf{k}_c) \rangle \\
&\quad + \frac{e}{4\hbar} \mathbf{B} \cdot \left[-iw(\mathbf{q}_c) \partial_{\mathbf{q}_c} \overline{w(\mathbf{q}_c)} + (A_n(\mathbf{k}_c) - \mathbf{r}_c) |w(\mathbf{q}_c)|^2 \right] \times \partial_{\mathbf{k}_c} \varepsilon_n(\mathbf{k}_c) + h.c. \tag{S7}
\end{aligned}$$

As the condition, $\langle W_n | \hat{\mathbf{r}} | W_n \rangle = \mathbf{r}_c$, imposes $iw(\mathbf{q}_c) \partial_{\mathbf{q}_c} \overline{w(\mathbf{q}_c)} = (A_n(\mathbf{k}_c) - \mathbf{r}_c) |w(\mathbf{q}_c)|^2$, we finally obtain

$$E_2 = -\frac{ie}{4\hbar} \mathbf{B} \cdot \langle \partial_{\mathbf{k}_c} u_n(\mathbf{k}_c) | \times [\varepsilon_n(\mathbf{k}_c) - H_{0\mathbf{k}_c}] | \partial_{\mathbf{k}_c} u_n(\mathbf{k}_c) \rangle + h.c.. \tag{S8}$$

Since this result holds for any wave packet with \mathbf{k}_c , \mathbf{k}_c can be replaced with \mathbf{k} . Hence, $E_2 = \boldsymbol{\mu}(\mathbf{k}) \cdot \mathbf{B}$ where the orbital magnetic moment is defined by

$$\boldsymbol{\mu}(\mathbf{k}) = -\frac{ie}{4\hbar} \langle \partial_{\mathbf{k}} u_n(\mathbf{k}) | \times [\varepsilon_n(\mathbf{k}) - H_{0\mathbf{k}}] | \partial_{\mathbf{k}} u_n(\mathbf{k}) \rangle + h.c., \tag{S9}$$

The z component of $\boldsymbol{\mu}(\mathbf{k})$ is identical to Eq. (S2).

Equipped with the above result, we now derive Eq. (5) of the main text from the orbital magnetic moment formula in Eq. (S2). While we are interested in the Landau level spreading of the flat band, let us assume that the flat band is the n -th band with

energy ε_0 . Then, Eq. (S2) becomes

$$\mu_n(\mathbf{k}) = \frac{e}{\hbar} \text{Im} \langle \partial_x u_n(\mathbf{k}) | [\varepsilon_0 - H(\mathbf{k})] | \partial_y u_n(\mathbf{k}) \rangle, \quad (\text{S10})$$

$$= \frac{e}{\hbar} \text{Im} \langle \partial_x u_n(\mathbf{k}) | \sum_l |u_l(\mathbf{k})\rangle \langle u_l(\mathbf{k})| [\varepsilon_0 - H(\mathbf{k})] \sum_m |u_m(\mathbf{k})\rangle \langle u_m(\mathbf{k})| \partial_y u_n(\mathbf{k}) \rangle, \quad (\text{S11})$$

$$= \frac{e}{\hbar} \text{Im} \sum_{l,m} [\varepsilon_0 - \varepsilon_m(\mathbf{k})] \langle \partial_x u_n(\mathbf{k}) | u_l(\mathbf{k}) \rangle \langle u_m(\mathbf{k}) | \partial_y u_n(\mathbf{k}) \rangle \delta_{lm}, \quad (\text{S12})$$

$$= \frac{e}{\hbar} \text{Im} \sum_m [\varepsilon_0 - \varepsilon_m(\mathbf{k})] \langle \partial_x u_n(\mathbf{k}) | u_m(\mathbf{k}) \rangle \langle u_m(\mathbf{k}) | \partial_y u_n(\mathbf{k}) \rangle, \quad (\text{S13})$$

where the completeness relation $I = \sum_m |u_m(\mathbf{k})\rangle \langle u_m(\mathbf{k})|$ is used. Without loss of generality, one can assume that $\varepsilon_0 = 0$. Then, by inserting Eq. (S13) into the Eq. (S1), we obtain

$$E_{n,B}(\mathbf{k}) = \varepsilon_n(\mathbf{k}) + \mu_n(\mathbf{k})B = \mu_n(\mathbf{k})B, \quad (\text{S14})$$

$$= -B \frac{e}{\hbar} \text{Im} \sum_m \varepsilon_m(\mathbf{k}) \langle \partial_x u_n(\mathbf{k}) | u_m(\mathbf{k}) \rangle \langle u_m(\mathbf{k}) | \partial_y u_n(\mathbf{k}) \rangle, \quad (\text{S15})$$

$$= -2\pi \frac{\phi}{\phi_0} \text{Im} \sum_m \varepsilon_m(\mathbf{k}) \langle \partial_x u_n(\mathbf{k}) | u_m(\mathbf{k}) \rangle \langle u_m(\mathbf{k}) | \partial_y u_n(\mathbf{k}) \rangle, \quad (\text{S16})$$

where A_0 is the area of the unit cell, $\phi = BA_0$, and $\phi_0 = h/e$. Finally, noting that the fidelity tensor is defined by

$$\chi_{ij}^{nm}(\mathbf{k}) = \langle \partial_i u_n(\mathbf{k}) | u_m(\mathbf{k}) \rangle \langle u_m(\mathbf{k}) | \partial_j u_n(\mathbf{k}) \rangle = A_i^{nm}(\mathbf{k})^* A_j^{nm}(\mathbf{k}), \quad (\text{S17})$$

we obtain

$$E_{n,B}(\mathbf{k}) = -2\pi \frac{\phi}{\phi_0} \frac{1}{A_0} \text{Im} \sum_{m \neq n} \varepsilon_m(\mathbf{k}) \chi_{xy}^{nm}(\mathbf{k}). \quad (\text{S18})$$

Since we assume that the flat band's energy is zero, one should interpret $\varepsilon_m(\mathbf{k})$ in Eq. (S18) as the energy of the m -th band with respect to the flat band energy.

Supplementary Note 2. Symmetry constraint on the Landau level spreading of flat band

In this Supplementary Note, we study the symmetry transformation of the modified band dispersion $E_{n,B}(\mathbf{k})$ and the fidelity tensor $\chi_{ij}^{nm}(\mathbf{k})$. Here, we use a compact notation which can be applied to both unitary and anti-unitary (anti)-symmetries. In this notation, any symmetry operation $\hat{\sigma}$ can be expressed by

$$U_\sigma(\mathbf{k}) \overline{H(\mathbf{k})}^s U_\sigma(\mathbf{k})^\dagger = p H(O_\sigma \mathbf{k}), \quad (\text{S19})$$

$$\mathfrak{g}_\sigma = (O_\sigma, s, p), \quad (\text{S20})$$

where $s = 0, 1$ and $p = \pm 1$. The bar notation denotes the complex conjugation, i.e., $\bar{x} = x^*$. For example, $\mathfrak{g}_\sigma = (\mathbb{1}, 0, -1)$ and $(-\mathbb{1}, 1, 1)$ correspond to chiral and time-reversal symmetries, respectively, where $\mathbb{1}$ denotes the identity matrix. First consequence of symmetry in Eq. (S20) is that the band structure is symmetric with respect to σ . Namely, $p\varepsilon(\mathbf{k})$ is the corresponding energy eigenvalue at $O_\sigma \mathbf{k}$ for an energy eigenvalue $\varepsilon(\mathbf{k})$ in the band structure. Furthermore, symmetry relations are imposed on the energy eigenstates as follows.

$$U_\sigma(\mathbf{k}) \overline{|u_m(\mathbf{k})\rangle}^s = |u_{m_\sigma}(O_\sigma \mathbf{k})\rangle B_\sigma(\mathbf{k})_{m_\sigma m} \quad (m \neq n), \quad (\text{S21})$$

$$U_\sigma(\mathbf{k}) \overline{|u_n(\mathbf{k})\rangle}^s = |u_n(O_\sigma \mathbf{k})\rangle e^{i\phi_n(\mathbf{k})}, \quad (\text{S22})$$

for dispersive bands m ($m \neq n$) and the flat band n , respectively. Here, the band indices are defined such that $\varepsilon_m(\mathbf{k}) = p\varepsilon_{m_\sigma}(O_\sigma \mathbf{k})$, and $B_\sigma(\mathbf{k})_{m_\sigma m}$ and $e^{i\phi_n(\mathbf{k})}$ are unitary and periodic in the Brillouin zone. With the symmetry transformation of energy eigenstates defined above in Eqs. (S21) and (S22), one can derive symmetry constraint on the modified band dispersion $E_{n,B}(\mathbf{k})$ and the fidelity tensor $\chi_{ij}^{nm}(\mathbf{k})$.

Symmetry constraint on the modified band dispersion $E_{n,B}(\mathbf{k})$

We recall the definition of modified band dispersion $E_{n,B}(\mathbf{k})$:

$$E_{n,B}(\mathbf{k}) = -2\pi \frac{\phi}{\phi_0} \frac{1}{A_0} \text{Im} \langle \partial_x u_n(\mathbf{k}) | H(\mathbf{k}) | \partial_y u_n(\mathbf{k}) \rangle. \quad (\text{S23})$$

Note that n -th band is an isolated flat band with $\varepsilon_n(\mathbf{k}) = 0$. Now, we study the symmetry transformation of $l_{ij}^n(\mathbf{k}) := \langle \partial_i u_n(\mathbf{k}) | H(\mathbf{k}) | \partial_j u_n(\mathbf{k}) \rangle$ by using Eq. (S22):

$$\begin{aligned} l_{ij}^n(O_\sigma \mathbf{k}) &= \left[\langle \partial_{\mathbf{k}'_i} u_n(\mathbf{k}') | H(\mathbf{k}') | \partial_{\mathbf{k}'_j} u_n(\mathbf{k}') \rangle \right]_{\mathbf{k}'=O_\sigma \mathbf{k}} \\ &= [O_\sigma]_{ii'} [O_\sigma]_{jj'} \partial_{i'} \left(e^{i\phi_n(\mathbf{k})} \overline{\langle u_n(\mathbf{k}) |}^s U_\sigma(\mathbf{k})^\dagger \right) \\ &\quad \times \left(p U_\sigma(\mathbf{k}) \overline{H(\mathbf{k})}^s U_\sigma(\mathbf{k})^\dagger \right) \partial_{j'} \left(e^{-i\phi_n(\mathbf{k})} U_\sigma(\mathbf{k}) \overline{|u_n(\mathbf{k})\rangle}^s \right) \\ &= p [O_\sigma]_{ii'} [O_\sigma]_{jj'} \overline{\langle \partial_{i'} u_n(\mathbf{k}) | H(\mathbf{k}) | \partial_{j'} u_n(\mathbf{k}) \rangle}^s \\ &= p [O_\sigma]_{ii'} [O_\sigma]_{jj'} \overline{l_{i'j'}^n(\mathbf{k})}^s. \end{aligned} \quad (\text{S24})$$

Hence, we obtain

$$\begin{aligned} E_{n,B}(O_\sigma \mathbf{k}) &= -2\pi \frac{\phi}{\phi_0} \frac{1}{A_0} \text{Im} \left[p [O_\sigma]_{xi} [O_\sigma]_{yj} \overline{l_{ij}^n(\mathbf{k})}^s \right] \\ &= -(-1)^s p ([O_\sigma]_{xx} [O_\sigma]_{yy} - [O_\sigma]_{xy} [O_\sigma]_{yx}) \times 2\pi \frac{\phi}{\phi_0} \frac{1}{A_0} \text{Im} l_{xy}^n(\mathbf{k}) \\ &= (-1)^s p \text{Det} O_\sigma E_{n,B}(\mathbf{k}). \end{aligned} \quad (\text{S25})$$

Note that $l_{xx}^n(\mathbf{k})$ and $l_{yy}^n(\mathbf{k})$ are real, thus $\text{Im} l_{xx}^n(\mathbf{k}) = \text{Im} l_{yy}^n(\mathbf{k}) = 0$. We remark two cases when the LLS is strongly constrained by symmetry. First, when $(-1)^s p = -1$ and $O_\sigma = \mathbb{1}$ are satisfied at the same time, the modified band dispersion $E_{n,B}(\mathbf{k}) = 0$ vanishes. Chiral symmetry C and space-time-inversion symmetry I_{ST} , characterized by $\mathfrak{g}_C = (\mathbb{1}, 0, -1)$ and $\mathfrak{g}_{I_{\text{ST}}} = (\mathbb{1}, 1, 1)$ respectively, belong to this case. The second case is when $(-1)^s p \text{Det} O_\sigma = -1$ and $O_\sigma \neq \mathbb{1}$. In this case, $E_{n,B}(O_\sigma \mathbf{k}) = -E_{n,B}(\mathbf{k})$ and this implies that the minimum and maximum values of LLS has the same magnitude but opposite in sign, i.e., $\max E_{n,B}(\mathbf{k}) = -\min E_{n,B}(\mathbf{k})$. Notable examples are time-reversal symmetry T and reflection symmetry R .

Symmetry constraint on $\chi_{xy}^{nm}(\mathbf{k})$

Although the symmetry analysis for the modified band dispersion $E_{n,B}(\mathbf{k})$ is sufficient for studying the Landau level spreading (LLS), the symmetry analysis for $\chi_{xy}^{nm}(\mathbf{k})$ provides some useful insights for understanding of the LLS as the inter-band coupling. From Eqs. (S21) and (S22), we obtain the relation between $\chi_{ij}^{nm}(\mathbf{k})$ and $\chi_{ij}^{nm\sigma}(O_\sigma \mathbf{k})$ where the band m and the band m_σ are related by the symmetry σ so that $\varepsilon_m(\mathbf{k}) = p \varepsilon_{m_\sigma}(O_\sigma \mathbf{k})$:

$$\begin{aligned} \chi_{ij}^{nm\sigma}(O_\sigma \mathbf{k}) &= \left[\langle \partial_{\mathbf{k}'_i} u_n(\mathbf{k}') | u_{m_\sigma}(\mathbf{k}') \rangle \langle u_{m_\sigma}(\mathbf{k}') | \partial_{\mathbf{k}'_j} u_n(\mathbf{k}') \rangle \right]_{\mathbf{k}'=O_\sigma \mathbf{k}} \\ &= [O_\sigma]_{ii'} [O_\sigma]_{jj'} \partial_{i'} \left(e^{i\phi_n(\mathbf{k})} \overline{\langle u_n(\mathbf{k}) |}^s U_\sigma(\mathbf{k})^\dagger \right) \\ &\quad \times \left(U_\sigma(\mathbf{k}) \overline{|u_m(\mathbf{k})\rangle}^s \langle u_m(\mathbf{k}) | U_\sigma(\mathbf{k})^\dagger \right) \partial_{j'} \left(U_\sigma(\mathbf{k}) \overline{|u_n(\mathbf{k})\rangle}^s e^{-i\phi_n(\mathbf{k})} \right) \\ &= [O_\sigma]_{ii'} [O_\sigma]_{jj'} \overline{\chi_{i'j'}^{nm}(\mathbf{k})}^s. \end{aligned} \quad (\text{S26})$$

Let us now apply Eq. (S26) to i) chiral symmetry C , ii) space-time-inversion symmetry I_{ST} , iii) a combined symmetry $C_{\text{ST}} = C \circ I_{\text{ST}}$ with C and I_{ST} , iv) time-reversal symmetry T , and v) reflection symmetry

i) Chiral symmetry C is characterized by $\mathfrak{g}_C = (O_\sigma, s, p) = (\mathbb{1}, 0, -1)$, and Eq. (S26) implies $\chi_{ij}^{nm\sigma}(\mathbf{k}) = \chi_{ij}^{nm}(\mathbf{k})$. Noting that $\varepsilon_m(\mathbf{k}) = -\varepsilon_{m_\sigma}(\mathbf{k})$, we obtain

$$\sum_{a=m, m_\sigma} \varepsilon_a(\mathbf{k}) \chi_{ij}^{na}(\mathbf{k}) = 0. \quad (\text{S27})$$

Thus, for each chiral-symmetric pair $|u_m(\mathbf{k})\rangle$ and $|u_{m_\sigma}(\mathbf{k})\rangle$, the contribution to the modified band dispersion $E_{n,B}(\mathbf{k})$ cancels out.

ii) Space-time inversion I_{ST} define by $\mathfrak{g}_{I_{\text{ST}}} = (\mathbb{1}, 1, 1)$ imposes the condition $\chi_{ij}^{nm\sigma}(\mathbf{k}) = (\chi_{ij}^{nm}(\mathbf{k}))^*$. In I_{ST} -symmetric

system, let us suppose non-degenerate band structure with band labeling $m = m_\sigma$ with $\varepsilon_m(\mathbf{k}) = \varepsilon_{m_\sigma}(\mathbf{k})$ for simplicity. Hence,

$$\varepsilon_m(\mathbf{k}) \text{Im} \chi_{ij}^{nm}(\mathbf{k}) = 0, \quad (\text{S28})$$

and contribution from each energy eigenstate $|u_m(\mathbf{k})\rangle$ vanishes.

iii) Let us consider $C_{\text{ST}} = C \circ I_{\text{ST}}$, a combination of chiral and space-time-inversion symmetries, characterized by $\mathfrak{g}_{C_{\text{ST}}} = (\mathbb{1}, 1, -1)$. For this symmetry, the condition $\chi_{ij}^{nm\sigma}(\mathbf{k}) = (\chi_{ij}^{nm}(\mathbf{k}))^*$ is imposed. This symmetry constraint is similar to I_{ST} -symmetric system, but now $\varepsilon_m(\mathbf{k}) = -\varepsilon_{m_\sigma}(\mathbf{k})$. Hence,

$$\sum_{\{\varepsilon_a(\mathbf{k}) > 0\}} \varepsilon_a(\mathbf{k}) \text{Im} \chi_{ij}^{na}(\mathbf{k}) = \sum_{\{\varepsilon_{\bar{a}}(\mathbf{k}) < 0\}} \varepsilon_{\bar{a}}(\mathbf{k}) \text{Im} \chi_{ij}^{n\bar{a}}(\mathbf{k}). \quad (\text{S29})$$

In this system, both energy eigenstates with positive and negative energy eigenvalues contribute to the LLS with the same sign. In the main text, we discuss the spin-orbit-coupled (SOC) Lieb model. This model possesses C_{ST} ,

$$C_{\text{ST}} H_{\text{socL}}(\mathbf{k}) C_{\text{ST}}^{-1} = -H_{\text{socL}}(\mathbf{k}) \quad \text{where} \quad C_{\text{ST}} = \text{Diag}(1, -1, 1) \mathcal{K}. \quad (\text{S30})$$

This symmetry leads to $\chi_{\text{socL},xy}^{\text{fb},+}(\mathbf{k}) = (\chi_{\text{socL},xy}^{\text{fb},-}(\mathbf{k}))^*$.

iv) Time-reversal symmetry T is characterized by $\mathfrak{g}_T = (-\mathbb{1}, 1, 1)$, and $\chi_{ij}^{nm\sigma}(-\mathbf{k}) = (\chi_{ij}^{nm}(\mathbf{k}))^*$ consequently. Noting that $\varepsilon_m(\mathbf{k}) = \varepsilon_{m_\sigma}(-\mathbf{k})$, we obtain

$$\varepsilon_m(\mathbf{k}) \text{Im} \chi_{ij}^{nm}(\mathbf{k}) = -\varepsilon_{m_\sigma}(-\mathbf{k}) \text{Im} \chi_{ij}^{nm\sigma}(-\mathbf{k}). \quad (\text{S31})$$

Thus, $E_{n,B}(\mathbf{k}) = -E_{n,B}(-\mathbf{k})$, and this implies $\max E_{n,B}(\mathbf{k}) = -\min E_{n,B}(\mathbf{k})$.

v) For a discussion on reflection symmetry R , we consider R_x , characterized by $\mathfrak{g}_{R_x} = (\text{Diag}(-1, 1), 0, 1)$, for convenience. R_x imposes $\chi_{ij}^{nm\sigma}(-k_x, k_y) = -\chi_{ij}^{nm}(\mathbf{k})$. Considering $\varepsilon_m(\mathbf{k}) = \varepsilon_{m_\sigma}(-k_x, k_y)$, we obtain

$$\varepsilon_m(\mathbf{k}) \text{Im} \chi_{ij}^{nm}(\mathbf{k}) = -\varepsilon_{m_\sigma}(-k_x, k_y) \text{Im} \chi_{ij}^{nm\sigma}(-k_x, k_y), \quad (\text{S32})$$

and $E_{n,B}(\mathbf{k}) = -E_{n,B}(-k_x, k_y)$. In similar to iv), we conclude that $\max E_{n,B}(\mathbf{k}) = -\min E_{n,B}(\mathbf{k})$.

Let us comment on the case where some bands are degenerate. When the band m is degenerate with other band(s), $\chi_{ij}^{nm}(\mathbf{k})$ or $\varepsilon_m(\mathbf{k}) \text{Im} \chi_{ij}^{nm}(\mathbf{k})$ alone is not gauge invariant. Let us suppose that the D number of bands, whose band indices are m_1, m_2, \dots, m_D , form a set of degenerate bands $\{m\}$, i.e., $(m_1, m_2, \dots, m_D) \in \{m\}$. Then, $\sum_{a \in \{m\}} \chi_{ij}^{na}(\mathbf{k})$ and $\sum_{a \in \{m\}} \varepsilon_a(\mathbf{k}) \text{Im} \chi_{ij}^{na}(\mathbf{k})$ are gauge invariant under the gauge transformation,

$$|u_{m_i}(\mathbf{k})\rangle \rightarrow |u_{m_j}(\mathbf{k})\rangle G_{m_j m_i}(\mathbf{k}) \quad (i, j = 1, 2, \dots, D), \quad (\text{S33})$$

where $G_{m_j m_i}(\mathbf{k})$ is D -by- D unitary matrix.

Supplementary Note 3. Landau level spreading of flat-band system with chiral symmetry

In this Supplementary Note, we discuss the LLS of flat-band system in the presence of chiral symmetry. As discussed in the main text and Supplementary Note 1, the LLS of chiral-symmetric system is forbidden in finite or all range of magnetic flux. First, let us discuss some properties of chiral-symmetric system in the zero magnetic flux. For chiral-symmetric Hamiltonian, the symmetry relation,

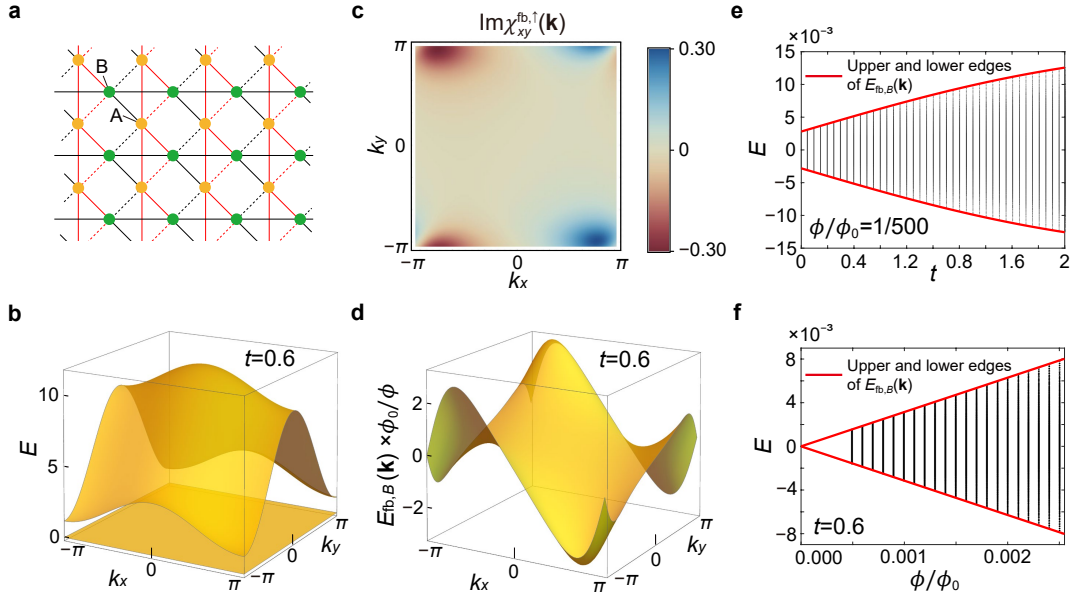
$$CH(\mathbf{k})C^{-1} = -H(\mathbf{k}) \quad (\text{S34})$$

holds. This implies that eigenstates $|u_a(\mathbf{k})\rangle$ and $|u_{\bar{a}}(\mathbf{k})\rangle$, having energy eigenvalues $\varepsilon_a(\mathbf{k})$ and $\varepsilon_{\bar{a}}(\mathbf{k}) = -\varepsilon_a(\mathbf{k})$ respectively, are related by the chiral symmetry operator C :

$$C|u_a(\mathbf{k})\rangle = |u_{\bar{a}}(\mathbf{k})\rangle B(\mathbf{k})_{\bar{a}a}. \quad (\text{S35})$$

Here, $B(\mathbf{k})$ denotes the sewing matrix for the chiral symmetry. The chiral eigenvalues c are given by the eigenvalues of $B_{\bar{a}a}(\mathbf{k})$. When $\varepsilon_{\bar{a}}(\mathbf{k}) = -\varepsilon_a(\mathbf{k}) \neq 0$, the sewing matrix is equal to

$$B(\mathbf{k})_{\bar{a}a} = \begin{pmatrix} 0 & 1 \\ 1 & 0 \end{pmatrix}, \quad (\text{S36})$$



Supplementary Figure 1. **Landau level spreading of a flat-band system with time-reversal symmetry.** **a** Lattice structure for the T -symmetric checkerboard model. Neighboring sites connected by the same type of bonds (a solid or dotted line) with the same color have the same hopping amplitudes. **b** The band structure of $H_T(\mathbf{k})$. **c** Distribution of $\text{Im}\chi_{xy}^{\text{fb},\uparrow}(\mathbf{k})$. **d** The modified band dispersion $E_{\text{fb},B}(\mathbf{k})$ of the flat band in the presence of magnetic flux. **e** Landau level spectra of the flat band (black dots) as a function of t for magnetic flux $\phi/\phi_0 = 1/500$. **f** Landau level spectra of the flat band (black dots) as a function of magnetic flux ϕ/ϕ_0 for $t = 0.6$. **e, f** The upper and lower bounds of Landau levels are equal in magnitude but opposite in sign.

up to unitary transformation, and its eigenvalues are given by $c = \pm 1$. Conversely, this implies that two degenerate flat-bands with zero energy having opposite chiral eigenvalues $c = \pm 1$ can be gapped under chiral-symmetric perturbations. However, a set of zero-energy flat bands cannot be gapped when all the chiral eigenvalues of such flat bands are equal. Since the sewing matrix $B(\mathbf{k})_{\bar{a}a}$ for all bands is identical to the chiral symmetry operator C up to unitary transformation, the minimum number of zero-energy flat bands, guaranteed to exist due to the chiral symmetry, is given by $|\text{Tr}[C]|$.

In the magnetic finite flux, the system still remains chiral symmetric. This is because chiral symmetry arises from a specific way of choosing the hoppings between the sublattices, and it is not changed by the Peierls substitution. For the magnetic unit cell q times larger than the original unit cell, the minimal number of flat bands are equal to $q|\text{Tr}[C]|$ where q is determined by the magnetic flux $\phi/\phi_0 = q_0 \frac{p}{q}$ ($q_0, p, q \in \mathbb{Z}$). Note that q_0 is a constant dependent on the gauge choice and the models. These zero-energy flat bands still have the same chiral eigenvalues, thus these are protected by chiral symmetry ($C_{\text{new}} = \bigoplus_{i=1}^q C$ now). Hence, unless a gap between zero-energy and non-zero-energy Landau levels closes as the magnetic flux increases, the LLS is forbidden even in the finite magnetic flux when the number of flat bands is $q|\text{Tr}[C]|$ at the zero magnetic flux. When such a gap closing occurs at $\phi/\phi_0 = \varphi_*$, the LLS can be finite for the magnetic flux larger than φ_* . Nevertheless, there must be at least the $q|\text{Tr}[C]|$ number of zero-energy Landau levels.

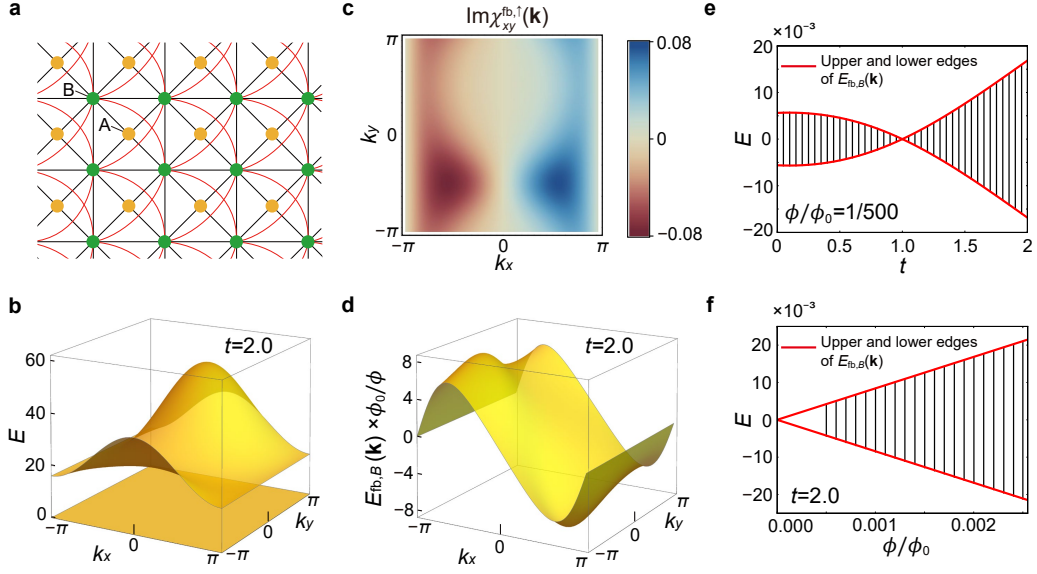
Supplementary Note 4. More lattice models

Time-reversal-symmetric system on the checkerboard lattice

When a time-reversal symmetry T exists at zero magnetic field, the LLS of an IFS has the minimum and maximum values of the same magnitude but opposite in sign. We consider a T -symmetric system defined in the checkerboard lattice. The lattice structure is shown in Supplementary Figure 1a. The on-site potentials at A- and B-sites are set to be 5 and $1 + t^2$, respectively. The hopping parameters are set to 2 along the red solid line, t along the black solid line, 1 along the red dashed lines, and $2t$ along the black dashed lines. The tight-binding Hamiltonian is written as

$$H_T(\mathbf{k}) = \begin{pmatrix} 5 + 4 \cos k_y & 2te^{-i\mathbf{k}\cdot\mathbf{d}_1} + 2e^{-i\mathbf{k}\cdot\mathbf{d}_2} + e^{i\mathbf{k}\cdot\mathbf{d}_1} + te^{i\mathbf{k}\cdot\mathbf{d}_2} \\ 2te^{i\mathbf{k}\cdot\mathbf{d}_1} + 2e^{i\mathbf{k}\cdot\mathbf{d}_2} + e^{-i\mathbf{k}\cdot\mathbf{d}_1} + te^{-i\mathbf{k}\cdot\mathbf{d}_2} & 1 + t^2 + 2t \cos k_x \end{pmatrix}, \quad (\text{S37})$$

where $\mathbf{d}_1 = (1/2, 1/2)$ and $\mathbf{d}_2 = (-1/2, 1/2)$. This Hamiltonian gives a zero-energy flat band, and a dispersive band with energy $\varepsilon_{T,\uparrow}(\mathbf{k}) = 6 + t^2 + 2t \cos k_x + 4 \cos k_y > 0$ as show in Supplementary Figure 1b. The time-reversal symmetry operator



Supplementary Figure 2. **Landau level spreading of a flat-band system with reflection symmetry.** **a** The lattice structure for the I_{ST} -symmetric checkerboard model. The red and black lines denote the hopping processes between A and B sublattices. **b** The band structure of $H_R(\mathbf{k})$ with $t = 2.0$. **c** Distribution of $\text{Im}\chi_{xy}^{\text{fb},\uparrow}(\mathbf{k})$ with $t = 2.0$. **d** The modified band dispersion $E_{\text{fb},B}(\mathbf{k})$ of the flat band in the presence of magnetic flux. **e** Landau level spectra of the flat band (black dots) as a function of t for magnetic flux $\phi/\phi_0 = 1/500$. We note that space-time inversion symmetry I_{ST} exist when $t = 1.0$, thus the LLS is strongly suppressed. **f** Landau level spectra of the flat band (black dots) as a function of magnetic flux ϕ/ϕ_0 for $t = 2.0$. **e, f** The upper and lower bounds of Landau levels are equal in magnitude but opposite in sign.

is given by the complex conjugation \mathcal{K} , i.e., $T = \mathcal{K}$, which gives a symmetry relation,

$$TH_T(\mathbf{k})T^{-1} = H_T(-\mathbf{k}). \quad (\text{S38})$$

The analytic form of the fidelity tensor $\chi_{xy}^{nm}(\mathbf{k})$ is given by

$$\chi_{xy}^{\text{fb},\uparrow}(\mathbf{k}) = \frac{(3 + 4i \sin k_y)(t^2 + 2i \sin k_x - 1)}{4(\varepsilon_{T,\uparrow}(\mathbf{k}))^2}. \quad (\text{S39})$$

Then, the modified band dispersion for the flat band is given by

$$E_{\text{fb},B}(\mathbf{k}) = -\frac{\pi(3t \sin k_x + 2(t^2 - 1) \sin k_y)}{\varepsilon_{T,\uparrow}(\mathbf{k})} \frac{\phi}{\phi_0}. \quad (\text{S40})$$

In Supplementary Figure 1c, d, $\text{Im}\chi_{xy}^{\text{fb},\uparrow}(\mathbf{k})$ and $E_{\text{fb},B}(\mathbf{k})$ are shown. Note that $E_{\text{fb},B}(-\mathbf{k}) = -E_{\text{fb},B}(\mathbf{k})$. Consequently, the Landau levels of the flat band spread in both positive and negative energy directions with the same amounts as shown in Supplementary Figure 1e, f.

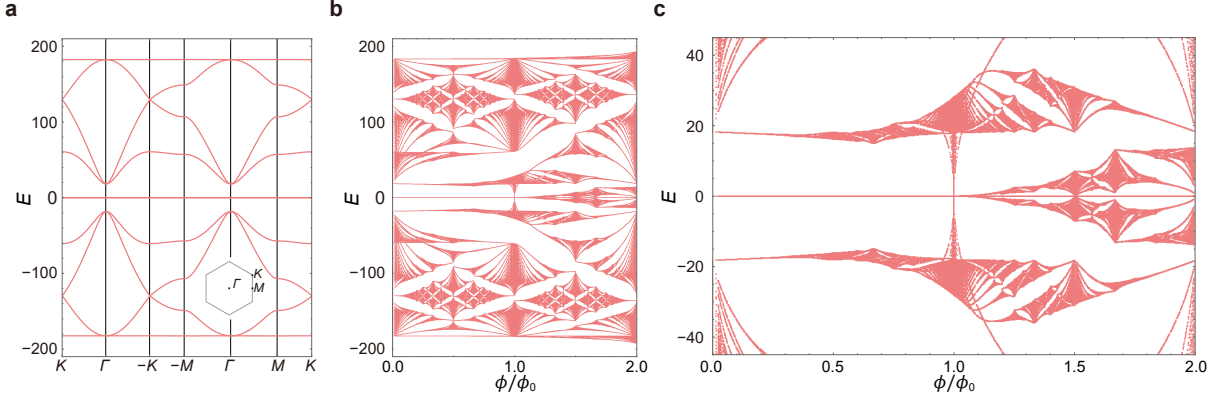
Reflection-symmetric system on the checkerboard lattice

In similar to time-reversal symmetric system at the zero magnetic field, we expect that the LLS whose the minimum and maximum values have the same magnitude but opposite in sign, for reflection R symmetric system at the zero field. We consider a R -symmetric system defined in the checkerboard lattice. This model is symmetric under reflection symmetry R in the x -direction. The lattice structure is shown in Supplementary Figure 2a. The tight-binding Hamiltonian consists of the hopping processes up to the next-to-next neighbor hopping. In momentum space, the Hamiltonian is written as

$$H_R(\mathbf{k}) = |\phi(\mathbf{k})\rangle\langle\phi(\mathbf{k})|, \quad (\text{S41})$$

$$|\phi(\mathbf{k})\rangle = (ie^{-i\mathbf{k}\cdot\mathbf{d}_1} + ie^{-i\mathbf{k}\cdot\mathbf{d}_2} + te^{i\mathbf{k}\cdot\mathbf{d}_1} + te^{i\mathbf{k}\cdot\mathbf{d}_2}, 4)^T, \quad (\text{S42})$$

where $\mathbf{d}_1 = (1/2, 1/2)$ and $\mathbf{d}_2 = (-1/2, 1/2)$. The band structure for $t = 2.0$ is shown in Supplementary Figure 2b. The flat



Supplementary Figure 3. **Landau level spreading of 10-band TBG model.** **a** The band structure for 10-band TBG model proposed in Ref. [30]. The Brillouin zone and the high-symmetry points are defined in the inset. **b** The Hofstadter spectrum exhibits the zero LLS of flat band at the magnetic flux ϕ/ϕ_0 in a range of $0 \leq \phi/\phi_0 < 1$. When $\phi/\phi_0 = 1$, a gap closing at $E = 0$ occurs, then the finite LLS is observed for $\phi/\phi_0 > 1$. **c** A zoom-in of the Hofstadter spectrum shown in **b**. Chiral symmetry guarantees the zero-energy Landau levels despite the appearance of non-zero LLS.

band's energy is zero and the energies of dispersive band is

$$\varepsilon_{R,\uparrow}(\mathbf{k}) = 18 + 2t^2 + 2(1 + t^2) \cos k_x + 4t \sin k_y + 2t \sin(k_x + k_y) - 2t \sin(k_x - k_y). \quad (\text{S43})$$

The reflection symmetry operator is given by $R = \text{Diag}(1, 1)$ which gives a symmetry relation,

$$RH_R(\mathbf{k})R^{-1} = H_R(-k_x, k_y). \quad (\text{S44})$$

The analytic form of the fidelity tensor $\chi_{xy}^{nm}(\mathbf{k})$ is given by

$$\chi_{xy}^{\text{fb},\uparrow}(\mathbf{k}) = \frac{8i \sin k_x (t^2 + 2i \cos k_y - 1)}{(\varepsilon_{R,\uparrow}(\mathbf{k}))^2}. \quad (\text{S45})$$

Then, the modified band dispersion for the flat band is given by

$$E_{\text{fb},B}(\mathbf{k}) = -\frac{16\pi(t^2 - 1) \sin k_x}{\varepsilon_{R,\uparrow}(\mathbf{k})} \frac{\phi}{\phi_0}. \quad (\text{S46})$$

In Supplementary Figure 2c, d, $\text{Im} \chi_{xy}^{\text{fb},\uparrow}(\mathbf{k})$ and $E_{\text{fb},B}(\mathbf{k})$ are shown. Note that $E_{\text{fb},B}(-k_x, k_y) = -E_{\text{fb},B}(\mathbf{k})$. Consequently, the Landau levels of the flat band spread in both positive and negative energy directions with the same amounts as shown in Supplementary Figure 2e, f.

Ten-band model for twisted bilayer graphene

In this Supplementary Note, we discuss one more example for chiral-symmetric system. For this, we consider the ten-band model for twisted-bilayer graphene (TBG) proposed in Ref. 30. The band structure and the Hofstadter spectrum is shown in Supplementary Figure 3a and 3b, c, respectively. The band structure exhibits two degenerate flat bands at zero energy when the on-site potential is neglected. Moreover, these flat bands have fragile topology protected by $C_{2z} \circ T$ [9, 10, 30, 57]. Although this system is not our interest in this paper as we focus only on an isolated and topologically trivial flat band, we study this system in detail as an important example of chiral-symmetric flat-band system.

As shown in Supplementary Figure 3b, c, There is no LLS in the Hofstadter spectrum for $0 \leq \phi/\phi_0 < 1$. This is because the chiral symmetry operator of this system is given by

$$C = \text{Diag}(-1, -1, -1, -1, 1, 1, 1, 1, 1, 1), \quad (\text{S47})$$

and $\text{Tr}[C] \neq 0$ at the zero magnetic field. According to the discussion in Supplementary Note 2, this implies the zero LLS in a finite range of the magnetic flux. Interestingly, the gap near $E = 0$ closes at $\phi/\phi_0 = 1$, and then the LLS is developed after the gap closing, as shown in Supplementary Figure 3c. The connection between the gap closing and fragile topology is discussed in Ref. 11.